ADDIS ABABA UNIVERSITY

A NEW METHOD OF NOTCHING IN VIBRATION CONTROL

by

Tollossa Deberie

A Thesis submitted to the School of Graduate Studies of Addis Ababa University in partial fulfilment of the requirements for the Degree of Masters of Science in Mechanical Engineering (Applied Mechanics stream)

Advisor

Dr. A.Raman

MECHANICAL ENGINEERING DEPARTMENT

ADDIS ABABA UNIVERSITY

OCTOBER 2007

ADDIS ABABA UNIVERSITY

SCHOOL OF GRAGUATE STUDIES

DEPARTEMENT OF MECHANICAL ENGINEERING

A New Method of Notching in Vibration Control

by

Tolossa Deberie

Approved by Board of Examiners:

Ato Hamsasew Moges

Chairman, Department Graduate Committee

Dr. A. Raman

Advisor

Dr. Abiy Aweke

External Examiner

Dr. Alem Bazezew

Internal Examiner

Date

Abstract

The traditional vibration test methodology of controlling the interface environment only to a motion based specification is often too conservative, inducing potentially excessive vibration responses at hardware resonant frequencies. This over testing problem occurs because the smooth, input acceleration specification used in the test configuration is characteristic of a rigid, infinite impedance equipment mount; and not characteristic of the compliant, finite impedance equipment mount more typical of the service configuration. Recently, the so called Force Limited Vibration (FLV) testing developed at the Jet Propulsion Laboratory offers many opportunities to decrease the over testing problem associated with traditional vibration testing. FLV testing methodology, controls the input acceleration and limits the reaction forces between the test item and the shaker through real-time notching of the input acceleration, is often hard subject to apply the force gauges. This problem has been recognized in this work and the energy limiting vibration test methodology has recently emerged as a viable solution which makes use of stress feedback signal to the vibration control loop using strain gauges that are trouble-free to the functions they are meant to perform. The underlying theoretical basis of the energy limiting vibration testing technique is the strain energy value which is the integration of product of von-mises stress and strain over an element is a parameter prime important since it is related to the total amount of energy transmitted to the test item during the vibration. To illustrate this methodology, a case study of a typical satellite presented to prove the effectiveness. A procedure was proposed to identify the topological location of notch channels or critical locations using FEM results of the base excitation, so as to enable the vibration control mechanism to adjust the power input of shaker table. The base excited dynamic response analysis yielded the percentage reduction of shaker power. The notching of the force limiting and energy limiting vibration testing methods were compared and founded incomparable even though it is acceptable.

Acknowledgements

First, many thanks to my advisor, Dr. A. Raman, for getting me started on the path that this research has taken. His inspiration and guidance through out the year has been invaluable in the conception and design of the new idea. I am looking forward to several more years of exploration and research under his guidance.

I would also like to thank the staffs of the department, both past and present. You have all endowed me with the knowledge and skill in my education in engineering from the beginning to this level and made this research successful.

In the faculty Library, I would also like to thank the staff as a whole for I got through all the materials the library has these two years and even got electronics library.

There are my class mates who I would like to thank for their conversations, support, and general friendship.

Finally, I would like to thank my entire friends, my family for encouraging me through these many years of school. They have all been a tremendous source of support and encouragement throughout all of this work. I appreciate their interest in my research.

Table of Contents

List of Tables

List of Figures

List of Symbols

Symbol	definition
A	interface accelerations
A_0	free acceleration of source
A_s	acceleration specification
F	interface force
F_s	force specification or limit
M_0	total mass
M	residual mass
$\underline{M}$	apparent mass F/A
Q	dynamic amplification factor
u	absolute displacement
U	generalized modal displacement
Φ	mode shape
ω	natural frequency
ω_0	natural frequency of uncoupled oscillator
ζ	the critical damping ratio
E	young's modulus
v	displacement vector
Y	normal coordinate
m	mass matrix
k	stiffness matrix
c	damping matrix
p	physical load
M	generalized (modal) mass matrix
K	generalized stiffness matrix
C	generalized damping matrix
P	generalized load
γ_i	participation factor
S_a	spectral acceleration
R_a	total modal response
ε	strain

Chapter One: Introduction

1.1 Background

Vibration testing is performed by applying known excitations to a test item and monitoring the response of the test item for subsequent analysis and evaluation. Vibration testing is commonly used in the design development, model validation, quality assurance, and qualification of products. Products include production machinery, ground vehicles, aircraft, space vehicles, household appliances, automatic weapon systems, control panels, measuring instruments, computer hardware, and nuclear power plant components.

Vibration tests are conducted in such a way that some tests are as simple as dropping the product from a certain height or loading it into the back of a truck and driving over the roughest roads in the area. However a lab tests for instance shaker tables which are usually faster, easier to instrument and more controllable are becoming inevitable. The basis for such vibration testing is closed loop control of vibratory excitation, more commonly known as vibration control; except these are more elaborate but as always, actual use or abuse will be the final test.

Typically for the qualification phase, most aerospace components have been submitted to the vibration qualification test; however, some components have showed structural failures during the vibrations, due to various reasons like: weak design, shaker hard-mounted test overloads (over testing), and unexpected hardware dynamics. Among all mentioned failure cases, this paper focuses on the case of component hard-mounted test overload reduction methods.

In vibration testing the test items are often over tested because of the discrepancies between the mechanical impedances and the force capabilities of the mounting structure and the vibration shaker and impossibility of simulating the actual vibration environment.
There is notching as an existing solution to the vibration over testing problem by the suppression of the drive signal in certain frequencies to respond to structure or system induced resonances in the control loop.

In tests without notching, the applied forces and responses are 3 to 10 times the maximum flight values for typical aerospace hardware. This test artifact is the cause of most vibration

test failures and is the driver of the design penalties for hardware which is designed to pass the test.

First a conventional vibration testing approach was developed for space hardware. This conventional approach of testing results in notches in the input acceleration based on the specifications of the acceleration input, namely, the envelope of the acceleration peaks of the flight environment, to the base of the test article. It has been known for decades to greatly over test the test item at its own resonance frequencies. Since space structures are designed to survive vibration testing as well as flight environment, this over testing phenomenon normally results directly in over design.

Where as the penalty of over testing in any case appears in design and performance compromises, as well as in the high costs and schedule overruns associated with recovery from artificial test failures that would have not occurred during the flight. In today's very competitive global market and better–cheaper–faster environment, there is a definite need for testing advanced space hardware with state-of-the-art technologies, instead of with the traditional approach with its very high design margin with respect to flight environment.

Later on an improved vibration test approach was developed and implemented at NASA's Jet Propulsion Laboratory (JPL), in the nineties. The approach is called force limited vibration (FLV) testing. In addition to controlling the input acceleration, the FLV testing measures and limits the reaction forces between the test item and the shaker through real-time notching of the input acceleration.

The problems involved in measuring base reaction forces on a shaker are common to force limited vibration tests. Most of these problems have been solved with the advent of commercially available three axis piezoelectric force gages and the associated signal conditioning equipment.

Yet the test fixturing to accommodate the force gages between the shaker and the test item remains a problem. Ideally, one would like to have no fixture mass between the gages and the test item, and this is possible when the gages may be simply used as a force washer with a longer than flight attachment bolt. In this case, the large dynamic range (typically - 60 dB) of the piezoelectric gages allows one to sense base reactions associated with the high frequency

resonances of very small masses on the test item. (The base reaction force falls off rapidly with increasing frequency.) The presence of an adapter plate above the force gages creates a wide band noise floor of force equal to the input acceleration times the adapter plate mass, below which test item forces may not be sensed.

A second problem with fixing concerns the need for a universal fixture incorporating force gages so that special fixturing need not be developed for each test. The use of the shaker armature current or a shaker fixture permanently incorporating force gages have been studied, but there are problems in subtracting out the force consumed by the armature and by the permanent fixturing, particularly when these are massive or flexible, compared to the test item.

A third problem concerns the inherent errors in force gage measurements. Experience with the three axis piezoelectric force gages indicates that most of these errors are small if the gage preloading is not exceeded and the surfaces mating to the gage are flat.

It should not be concluded that because of all the aforementioned problems, one cannot proceed with force limited vibration tests. On the contrary, over a dozen force limited vibration test projects involving flight hardware have been successfully conducted. It is the newness of the vibratory force measurement technology that makes it a hard subject of application. We argue that implementing an improved method of notching by shifting to other sensors that have simple and consistence application is vital.

1.2 Vibration Exciters

Vibration testing equipments are force generators or transducers that provide a vibration, shock or modal excitation source for testing and analysis. There are different types of vibration exciters: hammer, shaker table, etc. however this section deals with the shaker table.

Shaker Tables

Shaker tables are used to determine product or component performance under vibration or shock loads, detect flaws through modal analysis, verify product designs, measure structural fatigue of a system or material or simulate the shock or vibration conditions found in aerospace, transportation or other areas.

Shaker tables can operate under a number of different principles. Mechanical shakers use a motor with an eccentric on the shaft to generate vibration. Electrodynamic models use an electromagnet to create force and vibration. Hydraulic systems are useful when large force amplitudes are required, such as in testing large aerospace or marine structures or when the magnetic fields of electrodynamic generators cannot be tolerated. Pneumatic systems, known as "air hammer tables," use pressure air to drive a table. Piezoelectric shakers work by applying an electrical charge and voltage to a sensitive piezoelectric crystal or ceramic element to generate deformation and motion.

Common features of shaker tables are an integral slip table and active suspension. An integral slip allows horizontal or both horizontal and vertical testing of samples. The slip table is a large flat plate that rests on an oil film placed on a granite slab or other stable base. An active suspension system compensates for environmental or floating platform variations.

The three main test modes shaker tables can have are random vibration, sine wave vibration and shock or pulse mode. In a random vibration test mode, the force and velocity of the table and test sample will vary randomly over time. A sine wave test mode varies the force and velocity of the table and test sample sinusoidally over time. In a shock test mode, the test sample is exposed to high amplitude pulses of force.

The most important components for shaker tables which predict how the shakers are functioning are: shaker controllers, fixtures and instruments.

1.2.1 Shaker Controllers

Shaker controllers are hardware/software devices that generate one or more analog drive signals that are applied to an amplifier / shaker / test device for the purpose of creating a specified vibration environment at one or more points on a test device. The simplest types of shaker controllers are controlled manually and depend on the operator to read and evaluate the feedback signal and adjust the amplifier signal input voltage accordingly. This type of system can be as simple as a sine wave signal generator and an accelerometer monitored by a voltmeter. It is left to the operator to manually make the necessary gain compensation for changes in frequency or desired level specifications.

More complex units will feature automatic servo controlled levels with programming and frequency sweep capabilities. Top end controllers utilizing computer technology are available and can control to almost any specification with multiple accelerometers, etc.

The most critical specifications for shaker controllers are number of inputs and outputs, output dynamic range and frequency range, and what types of testing the user needs performed. The types of tests include simple outputs such as a random Gaussian output signal, classical shock and arbitrary transients. More complex signals are available as well. Sine on random is a test signal in which narrowband sine waves are combined with broadband random waves for a complex vibration signal. Random on random produces a test signal that has narrowband random waves combined with broadband random waves. A shock response system calculates the responses of a large number of theoretical, single-degree-of-freedom spring-mass systems to a given shock pulse.

The Essence of Vibration Controller

1. User defines his vibration test requirement by entering his data into the vibration controller. This defines the frequency and amplitude content of the required vibration.
2. The vibration controller produces an initial drive signal.
3. The signal is amplified by a power amplifier that drives a shaker. An electro-dynamic shaker operates over a wider frequency range than a hydraulic shaker but a hydraulic shaker is capable of more force and displacement.
4. The unit under test (UUT) or test item is mounted on the shaker table. The vibration on the shaker table is measured using an accelerometer whose signal is fed back to the vibration controller.
5. A control algorithm within the controller computes the transfer function of the closed loop system and hence corrects the output drive signal such that the vibration on the shaker table matches the user defined frequency and amplitude specification.

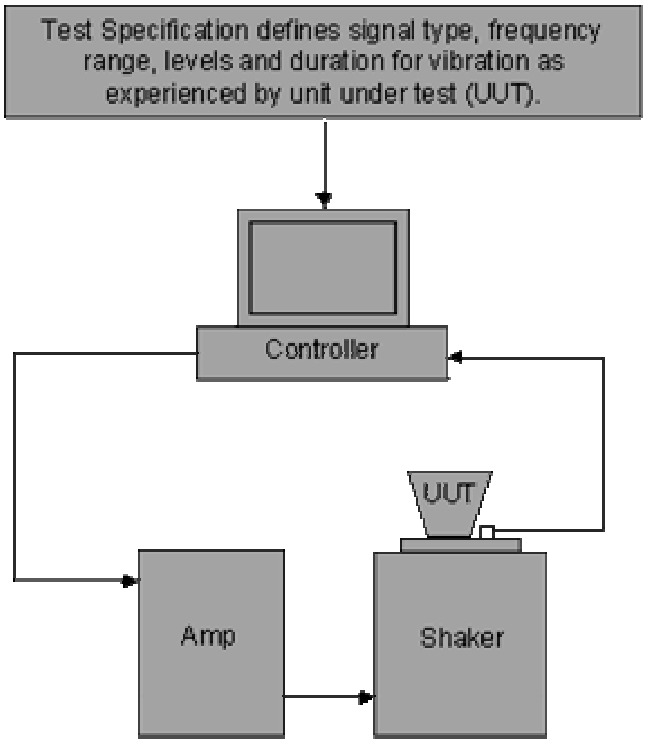

Figure 1-1 Vibration Control Setup

1.2.2 Vibration Test Fixture

A Vibration test fixture is a device that typically interfaces the vibration shaker table and the test item. It's adapted for attachment to a conventional shaker table to support a test item relative to the shaker table so that the test item can be vibrated along three mutually orthogonal axes in a single vibration test procedure without repositioning the test item during the procedure. This fixture shall simultaneously apply three equal mutually orthogonal X, Y and Z axes by a single attachment of the test item to the test fixture.

The test fixture is comprised of a flat plate assembly which has a bottom edge and a support structure. The support structure is designed to support the test item in a selected fixed relationship to the vertical or horizontal vibration input. The test item, as secured to the support structure, is inclined at an angle with respect to the mounting surface of the vibration shaker. As a result of this inclination, the Z axis of the test item is also inclined. By rotating the test item on the inclined flat plate, each of the three equal, mutually orthogonal vibration force components of the input vibration force will extend along the corresponding X, Y and Z axes of the test item with one exposure instead of three separate exposures resulting in significant labour and time savings.

The 3 axis Vibration Fixture may be designed to accommodate test items of varying sizes and payloads. The fixture is constructed of materials that insure the lightest possible weight and is a weldment to provide the optimum in strength and rigidity.

Fixture Design

Its design may range from a very simple plate with a few attachment holes to an extremely complex device either designed specifically for a unique test item or designed with automatic features which allow production testing to occur with the rapid insertion and/or removal of the test item.

Often, for products which do not exhibit any unique mounting characteristics, a universal style fixture is appropriate. Fixtures of this type may be classified as Cube, L or T.

In the case of the cube fixture, there would be 5 faces available to mount test items as the bottom surface would be hard mounted to the test apparatus and not available to mount test item. If the condition of test is to vibrate in each of three mutually orthogonal axes, the cube lends itself as the perfect fixture. One may place product on the top surface as axis Z and on each of the sides for axes X and Y. It would only be required to rotate the test item in relation to each face of the cube to realize all the orthogonal axes. Assuming the test equipment could handle the resulting payload, the cube fixture is capable of testing up to 5 products at a time, thereby minimizing total test time.

For those with 6 axes requirements, a cube may be fabricated with a cavity on the top such that the test item may be situated inside the cube while mounted on an adapter plate for the –Z axis.

The L and T Fixtures are particularly useful in supplying a mounting surface perpendicular to the direction of the test apparatus. The product may be mounted directly to the apparatus for one orthogonal axis, but if for some technical reason, the product does not allow itself to be mounted on its side relative to the position of the apparatus, an L or T fixture would be appropriate. The product would be mounted on the vertical member of the L or T for the second axis and then rotated 90 degrees in order to perform the third axis. Note that the vertical member of the T fixture may accept product on either side to maximize test throughput.

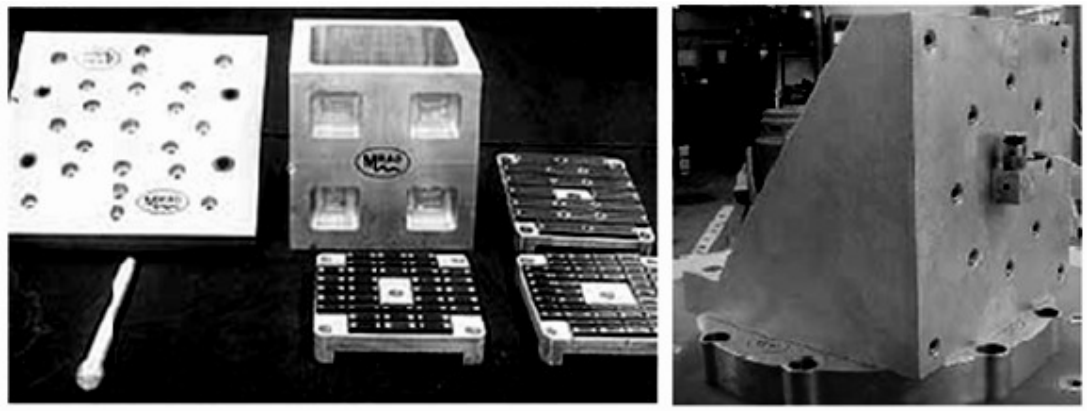

Figure 1-2 Cubic and "L" fixtures

1.2.3 Instrumentation

Herein are described the characteristics and use of piezo-electric force transducers and other instrumentation employed in vibration testing.

1.2.3.1 Piezo-electric Force Transducers

The use of piezo-electric force transducers for force limited vibration testing is highly recommended over other types of force measurement means such as strain transducers, armature current, weighted accelerometers, etc.

The high degree of linearity, dynamic range, rigidity, and stability of quartz make it an excellent piezo-electric material for both accelerometers and force transducers martini [7]. Similar signal processing, charge amplifiers and voltage amplifiers, may be used for piezo-electric force transducers and accelerometers. However, there are several important differences between these two types of measurement. Force transducers must be inserted between (in series with) the test item and shaker and therefore they require special fixtures, whereas accelerometers are placed upon (in parallel with) the test item or shaker. The total force into the test item from several transducers placed at each shaker attachment may be obtained by simply using a junction to add the charges before they are converted to voltage. On the other hand, the output of several accelerometers is typically averaged rather than summed. Finally, piezo-electric force transducers tend to put out more charge than piezo-electric accelerometers because the force transducer crystals experience higher loading forces,

so sometimes it is necessary to use a charge attenuator between the force transducer and the charge amplifier.

Force Transducer Preload

Piezo-electric force transducers must be preloaded so that the transducer always operates in compression. The transverse forces are carried through the force transducer by friction forces. These transverse forces act internally between the quartz disks inside the transducer as well as between the exterior steel disks and the mating surfaces. Typically the maximum transverse load is 0.2, the coefficient of friction, times the compressive preload. Having a high preload, and smooth transducer and mating surfaces, also minimizes several common types of transducer measurement errors, e.g. bending moments being falsely sensed as tension/compression if gapping occurs at the edges of the transducer faces. However, using flight hardware and fasteners, it is usually impossible to achieve the manufacturers recommended preload, so some calculations are necessary to insure proper performance. Sometimes it is necessary to trade-off transducer capability for preload and dynamic load. (This is often the case if there are large dynamic moments which can't be eliminated by designing the fixtures to align the load paths.) The three requirements for selecting the preload are: 1. it must be sufficient to carry the transverse loads through the transducer by friction, 2. it must be sufficient to prevent loss of compressive preload at any point on the transducer faces due to the dynamic forces and moments, and 3. it must be limited so that the maximum stress on the transducer does not exceed that associated with the manufacturer's recommended maximum load configuration.

Transducer preloading is applied using a threaded bolt or stud which passes through the inside diameter of the transducer. With this installation, the bolt or stud acts to shunt past the transducer a small portion of any subsequently applied load, thereby effectively reducing the transducer's sensitivity. Calibration data for the installed transducers is available from the manufacturer if they are installed with the manufacturer's standard mounting hardware. Otherwise, the transducers must be calibrated in situ as discussed in the next section.

Force Transducer Calibration

The force transducer manufacturer provides a nominal calibration for each transducer, but the sensitivity of installed units depends on the size and installation of the bolt used for preloading and therefore must be calculated or measured in situ. This may be accomplished

either quasi-statically or dynamically. Using the transducer manufacturer's charge amplifiers and a low noise cable, the transducers will hold their charge for many hours, so that it is possible to calibrate them statically with weights or with a hydraulic loading machine. If weights are used, it is recommended that the calibration be performed by loading the transducers, re-setting to short-out the charge, and then removing the load, in order to minimize the transient overshoot.

The simplest method of calibrating the transducers for a force limited vibration test is to conduct a preliminary low-level sine sweep or random run and to compare the apparent mass measured at low frequencies with the total mass of the test item. The appropriate apparent mass is the ratio of total force in the shaker direction to the input acceleration. The comparison must be made at frequencies much lower than the first resonance frequency of the test item. Typically the measured force will be approximately 80 to 90% of the weight in the axial direction and 90 to 95% of the weight in the lateral directions, where the preloading bolts are in bending rather than in tension or compression. Alternately, the calibration correction factor due to the transducer preloading bolt load path may be calculated by partitioning the load through the two parallel load paths according to their stiffness; the transducer stiffness is provided by the manufacturer, and the preload bolt stiffness in tension and compression or bending must be calculated. (The compliance of any structure in the load path between the bolt and transducer must be added to the transducer compliance.)

1.2.3.2 Strain Gages

Strain gages are the most common sensing element to measure surface strain.

Structure of Strain Gages

There are many types of strain gages. Among them, a universal strain gage has a structure such that a grid-shaped sensing element of thin metallic resistive foil (3 to 6μm thick) is put on a base of thin plastic film (15 to 16μm thick) and is laminated with a thin film.

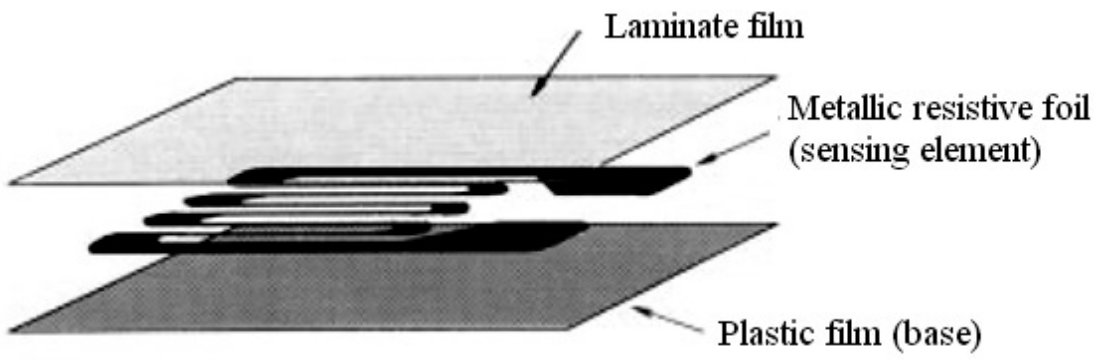

Figure 1-3 Structure of Strain Gages

Principle of Strain Gages

The strain gage is tightly bonded to a measuring object so that the sensing element (metallic resistive foil) may elongate or contract according to the strain borne by the measuring object. When bearing mechanical elongation or contraction, most metals undergo a change in electric resistance. The strain gage applies this principle to strain measurement through the resistance change. Generally, the sensing element of the strain gage is made of a copper-nickel alloy foil. The alloy foil has a rate of resistance change proportional to strain with a certain constant.

Let's express the principle as follows:

$$\frac{\Delta R}{R} = K.\varepsilon \tag{1.1}$$

where, R: original resistance of strain gage, Ω(ohm)

ΔR: elongation- or contraction-initiated resistance change,

K: proportional constant (called gage factor),

ε: strain.

The gage factor, K differs depending on the metallic materials. The copper-nickel alloy (Advance) provides a gage factor around 2. Thus, a strain gage using this alloy for the sensing element enables conversion of mechanical strain to a corresponding electrical resistance

change. However, since strain is an invisible infinitesimal phenomenon, the resistance change caused by strain is extremely small.

Types of Strain Measuring Methods

There are various types of strain measuring methods, which may roughly be classified into mechanical, optical, and electrical methods. Since strain on a substance may geometrically be regarded as a distance change between two points on the substance, all methods are but a way of measuring such a distance change. If the elastic modulus of the object material is known, strain measurement enables calculation of stress. Thus, strain measurement is often performed to determine the stress initiated in the substance by an external force, rather than to know the strain quantity.

Strain Measurement with Strain Gages

Since the handling method is comparatively easy, a strain gage has widely been used, enabling strain measurement to imply measurement with a strain gage in most cases. When a fine metallic wire is pulled, it has its electric resistance changed. It is experimentally demonstrated that most metals have their electrical resistance changed in proportion to elongation or contraction in the elastic region. By bonding such a fine metallic wire to the surface of an object, strain on the object can be determined through measurement of the resistance change. The resistance wire should be 1/50 to 1/200mm in diameter and provide high specific resistance. Generally, a copper-nickel alloy (Advance) wire is used. Usually, an instrument equipped with a bridge circuit and amplifier is used to measure the resistance change. Since a strain gage can follow elongation/contraction occurring at several hundred kHz, its combination with a proper measuring instrument enables measurement of impactive phenomena. Measurement of fluctuating stress on parts of running vehicles or flying aircraft was made possible using a strain gage and a proper mating instrument.

1.3 Thesis Objectives

The general objective of this thesis is to develop an effective new method of vibration testing control specification of a shaker enhancing the existing vibration control methods. The following are the main objectives of the thesis:

1. To develop a new method energy limited vibration testing method
2. To develop an FE model of typical satellite to illustrate the effectiveness of the method.

3. To analyze statically the satellite to demonstrate the model is safe statically
4. To analyze the mode shape in order to determine the effective mass of the model
5. To determine the energy limitation (specification) of the base exited dynamic response of the model
6. To determine the percentage reduction of shaker power

For these, ANSYS is used for parametric modelling, for meshing and is used as solver.

1.4 Thesis Statement

The thesis is a presentation of a new contribution involving energy limiting approach. It argues that considerable advantages can be obtained by the make use of stress feedback signal to the vibration control loop using strain gauges that are trouble-free to the functions they are meant to perform. Although recently most vibration testing is dedicated to aerospace industry manipulating Force Limited Vibration (FLV) method, force gauge are difficult to implement efficiently in vibration testing. This sensor is new, as is the exploration of the vibration method. The thesis proposes the existence of a promising method, demonstrating its generality, usefulness and application to vibration testing tasks.

In this research investigation a procedure will be proposed to identify the topological location of notch channels using FEM results, so as to enable the servo control mechanism to adjust the power input of shaker vibration table. Based on this methodology a case study of a typical satellite will be investigated to prove the effectiveness. The base excited dynamic response analysis will yield the percentage reduction of shaker power.

1.5 Thesis Organization

The report consists of seven chapters, first being introduction. In second chapter, literature review of various literatures on the vibration testing control is carried out. Third chapter depicts the basic conceptual foundation in vibration testing and impedance. In chapter four, the theory of vibration superposition is defined for frequency and time domain. Chapter five deals with the description of satellite structure, Finite Element model of the satellite structure and it contains the steps followed in static and spectral analysis of the model of the problem on ANSYS software. In chapter six the results obtained by FEM and analytically are discussed. Chapter seven concludes with the conclusion & scope for future work.

Chapter Two: Literature Review

With the arrival of many researchers from 1950s to reduce the over testing of test specimen on a shaker table had made an improved different vibration testing approach based on measuring and limiting the response motion or reaction force between the shaker and structure. This chapter tries to summarize some key background references and their contributions to the problem of over testing.

Formerly Blake [1] describes the problem of over testing at resonances of the test piece, which results from the standard practice of enveloping the peaks in the field acceleration spectral data, for both vibration and shock tests. He proposed a complex, conceptual solution in which the impedance of the mounting structure would be simultaneously measured with a small shaker and emulated by the test shaker. After a few years Morrow [2] warned against ignoring "mounting structure impedance" in both vibration and shock tests and shows that impedance concepts familiar to electrical engineers are largely unknown to mechanical engineers. He describes exact impedance simulation using force transducers between the shaker and test structure, but points out the difficulties in simulating impedance exactly, because of angle. Phase angle is impractical to specify and control the shaker impedance exactly. Moreover to integrate the theory of impedance to vibration testing, O'Hara [3] and Rubin [4] in two complementary papers translate and extend the electrical engineering impedance concepts into mechanical engineering terms. O'Hara points out an important distinction between impedance, the ratio of force to an applied velocity, and mobility, the ratio of velocity to an applied force. Rubin developed transmission-matrix concepts, which are very useful for coupling systems together and for analyzing vibration isolation.

The major break through to the development of vibration testing was the advancement of vibration testing shakers, shaker fixtures, sensors, and so on. For instance, Ratz [5] designs and tests a new shaker equalizer, which uses force feedback to simulate the mechanical impedance of the equipment mounting structure (foundation). Later Scharton [6] develops special, multi-modal, vibration test fixtures, which had enhanced modal densities and low rigidities, to mechanically simulate the impedance of large flight mounting structures. Subsequently Martini [7] describes the use of the piezo-electric, quartz, multi-component force transducer, which is certainly the most important enabling factor in making force limited vibration testing a reality.

Earlier weak methods of force limiting had been known to be used. It follows that Salter [8] calls for two test improvements to alleviate over testing: 1) multi-point control to reduce the impact of fixture resonances and 2) force limiting to account for the vibration absorber effect at test item resonances. He proposes a very simple method of computing the force limit, i.e. the force is limited to 1.5 times the mass times the peak acceleration, i.e. the acceleration specification. His approach, in conjunction with a review of the force data obtained in the system acoustic tests of the Cassini spacecraft, provides the impetus for what in this paper is called the semi-empirical method of predicting force limits.

For another class of problems, Heinricks [9] and McCaa and Matrullo [10] discuss on the analysis and test, respectively, of a lifting body re-entry vehicle using force limiting to notch a random vibration acceleration spectrum. A complete modal model including the effective mass concepts discussed herein, are developed in the analysis. The analysis also includes a comprehensive finite element model (FEM) simulation of the force limited vibration test, in which the test input forces are limited to the structural limit-load criteria. A vibration test of a scale model vehicle is conducted using single-axis impedance-head force transducers to measure the total force input, and the notching is implemented manually based on force data from low level tests. In addition at the same year Painter [11] conducts an experimental investigation of the sinusoidal vibration testing of aircraft components using both force and acceleration specifications. The interface forces and accelerations between simulated equipment and an aircraft fuselage were measured and enveloped, and these envelopes are used to control shaker sinusoidal vibration tests of the equipment. It is found that the procedure largely eliminated the high levels of over testing introduced by the conventional approach.

In a similar manner to the semi-empirical method Murfin [12] develops the concept of dual control, the first of several at Sandia National Laboratories to contribute to the technology of force limiting. He proposes that a force specification be developed and applied in a manner completely analogous to the acceleration specification. He proposes a method of deriving the forces from the product of the acceleration specification and the smoothed apparent mass of the test item. However he ignores the mounting structure impedance. Witte and Rodman [13] and Hunter and Otts [14] continue to pursue the calculation of the force specification by multiplying the acceleration specification times the smoothed apparent mass of the test item. They use (Similar to Murfin et al ignore the mounting structure impedance) simple parametric

models to interpret field data and to study the dynamic absorber effect of the payload at resonance, and develop special methods of smoothing the test item apparent mass.

Alternately Witte [15] proposes a method of controlling the product of the force and acceleration, which is applicable when no information is available on either the test piece or the mechanical impedance of mounting structure.

Moreover Wada, et al [16] develop a technique for obtaining an equivalent single-degree-of-freedom system (SDFS) for each eigen-vector when the dynamic characteristics of the structure are available in the form of a finite element model (FEM) or as test data. In addition Sweitzer [17] develop a very simple method of correcting for mechanical impedance effects during vibration tests of typical avionics electronic equipment. In essence, the method is to let the test specimen have a resonance amplification factor of only the square root of Q, rather than Q as it would on a rigid foundation. This is implemented in the test by notching the input acceleration by the same factor, i.e. the square root of Q.

In a study of quantifying the degree of over testing in conventional aerospace vibration tests, Judkins and Ranaudo [18] conduct a definitive series of tests. Their objective is to compare the damage potential of an acoustic test and a conventional random vibration test on a shaker. The study shows that the shaker resulted in an over test factor (ratio of shaker to acoustic test results) of 10 to 100 for peak spectral densities and a factor of ten for g rms's. They point out that significant savings in design schedules and component costs will result from reduced vibration test levels, which are developed by taking into account the compliance of the mounting structure in the vibration tests of spacecraft components. Also Piersol, et al. [19] conduct a definitive study of the causes and remedies for vibration over testing in conjunction with Space Shuttle Sidewall mounted components. One aspect of their study is to obtain impedance measurements on the shuttle sidewall and correlate the data with FEM and semi-empirical models. They propose as a force limit the "blocked force", which is the force that the field mounting structure and excitation would deliver to a rigid, infinite impedance, load.

In an exceptional research Scharton and Kern [20] propose a dual control vibration test in which both the interface acceleration and force are measured and controlled**.** They derive an exact dual control equation, which relates the interface acceleration and force to the free acceleration and blocked force. Alternately, they propose an approximate relationship, for

dual extremal control, in which the exact relation is replaced by extremal control of the interface acceleration to its specification and the interface force to its specification.

Furthermore Scharton, et al. [21] describe a dual controlled vibration test of aerospace hardware, a camera for the Mars Observer spacecraft, using piezo-electric force transducers to measure and notch the input acceleration in real time. Since the controller would not allow a separate specification for limiting the force, it was necessary to use a shaping filter to convert the force signal into a pseudo-acceleration. One of the lessons learned from this project was that the weight of the fixture above the force transducers should represent a small fraction (less than 10%) of the test specimen weight. In another independent study, Scharton [22] analyzes dual control of vibration testing using a simple two degree-of-freedom system. The study indicates that dual controlled vibration testing alleviates over testing, but that the blocked force is not always appropriate for the force specification. An alternative method is developed for predicting a force limit, based on random vibration parametric results for a coupled oscillator system described in the literature.

From JPL, Scharton [23] describes testing of nine flight hardware projects, one of which is the complete TOPEX spacecraft tested at NASA Goddard Space Flight Center. Two of the cases include validation data, which show that the force limited vibration test of the components, are still conservative compared with the input data obtained from vibration tests and acoustic tests at higher levels of assembly. Later Scharton [24] describes two applications of force limiting: the first to the Wide Field Planetary Camera II for the first Hubble telescope servicing mission, and the second to an instrument on the Cassini spacecraft. He pointed out that there are many approaches to denying a force specification and new and better methods are certain to evolve.

Immediately afterwards Scharton [25] devises a method of calculating force limits by evaluating the test specimen dynamic mass at the coupled system resonance frequencies. Application of the method to a simple or a complex coupled oscillator system yields non-dimensional analytical results which may be used to calculate limits for future force limited vibration tests. The analysis for the simple system provides an exact, closed form result for the peak force of the coupled system and for the notch depth in the vibration test. The analysis for the complex system provides parametric results, which contain both the effective modal

and residual masses of the test specimen and mounting structure, and is therefore well suited for use with FEM models.

In yet another study Scharton and Chang [26] do the application of force limited vibration testing by describing the force limited vibration test of the Cassini spacecraft conducted in November of 1996. Over a hundred acceleration responses were monitored in the spacecraft vibration test, but only the total axial force is used in the control loop to notch the input acceleration. They concluded that the instrument force limits derived with the semi-empirical method are generally equal to or less than those derived with the two-degree-of-freedom method, but are still conservative with respect to the interface force data measured in the acoustic test. In a similar manner McNelis and Scharton [27] deal with Force limited random vibration testing at NASA John Glenn Research Center for qualifying aerospace hardware for flight. They describe that the benefit of force limiting testing is that it limits over testing of flight hardware, by controlling input force and acceleration from the shaker (dual control) to the test structure. This paper also addresses recent flight camera testing (qualification random vibration and strength testing) for the Combustion Module-2 mission and the impact of Semi-empirical Method force limits.

Smallwood [28] contributed by conducting an analytical study of a vibration test method using extremal control of acceleration and force. He finds that the method limited the acceleration input at frequencies where the test item responses tend to be unrealistically large, but that the application of the method is not straightforward and requires some care. He concluded that the revival of test methods using force is appropriate considering the advances in testing technology in the last fifteen years, and that the method reviewed shows real merit and should be investigated further. Moreover Smallwood [29] establishes a procedure to derive an extremal control vibration test based on acceleration and force, which can be applied to a wide variety of test items. This procedure provides a specific, justifiable way to notch the input based on a force limit.

Recently for deriving the force specification Stevens [30] developed a vibration testing techniques that reduce the over testing caused by the essentially infinite mechanical impedance of the shaker in conventional vibration tests. He proposed a new method of deriving the force specification that is based on a modal method of coupling two dynamic systems, in this case “source” or launch vehicle, and the “load” or payload. The only

information that is required is an experimentally-measurable frequency-response function (FRF) called the dynamic mass for both the source and the load. The method, referred to as the coupled system, modal approach (CSMA) method, is summarized and compared to an existing method of determining the force specification for force-limited vibration testing.

Daniel B. and Worth [31] deal with the latest force-limited control techniques for random vibration testing by the implementation of force-limited vibration control on a controller which can only accept one profile. The method uses a personal computer-based digital signal processing board to convert force and/or moment signals into what appears to be an acceleration signal to the controller. The paper describes the method, hardware, and test procedures used. An example from a test performed at NASA/GSFC is used as a guide.

In the development of the force limited method in late 1990's Worth and Kaufman [32] describe the validation of the force-limited testing approach for random vibration testing on a sounding rocket experiment. A simple structure was flown and instrumented with accelerometers and force gages. The results of the data acquired during the flight test are compared with predicted results which were performed prior to the flight tests and the data are used for the validation. Additionally, the data will be used for others to develop improved analytical techniques for force-limited vibration testing. Subsequently Amato, et al. [33] deal with the acceleration controlled and force limited vibration testing of the HESSI imager flight unit. They describe that the force limited strategy successfully survived the vibration testing of the imager by reducing the shaker force and notching the acceleration at resonances. The test set-up, test levels, and results are presented. They also discussed the development of the force limits.

Again Chang [34] deals with the force-limited random vibration test in two axes for the environmental qualification program for the Deep Space 1 spacecraft. He used a semi-empirical force limit procedure to derive force limits for the test and therefore the results of the test show that the acceleration inputs measured near the feet of a number of spacecraft mounted instruments reached their assembly random vibration test specifications. Also, several major structural elements of the spacecraft reached their flight limit loads during the spacecraft vibration test.

The traditional vibration testing established on motion specification yet again was carried out as Ceresetti [35] deals with a dedicated vibration test technique, *response limiting*, which limits the random vibration response induced in the test item by the shaker, and states that it has been successful for the qualification test of the Duct Smoke Detector (DSD) for the Multi Purpose Logistics Module (MPLM) and Columbus Orbital Facility (COF) projects of the International Space Station (ISS). He describes that the approach serves to eliminate unrealistic resonance acceleration loads that are induced by the shaker on the test item and therefore provides more realistic "in-flight-like" conditions.

With the use of a new Force Measurement Device (FMD), to measure directly the forces and moments at the spacecraft/launch-vehicle interface, Salvignol and Brunner [36] conduct a sine-vibration testing of European Space Agency's (ESA) Rosetta spacecraft. The Device proved extremely useful in ensuring that the test levels required by the launcher authorities were strictly applied, and that the tests were executed safely. The FMD's output was also valuable for the validation of the finite-element model and therefore the use of this new device, is highly recommended in conducting future spacecraft qualification and acceptance vibration tests.

In line with all the existing methodology, Spanos and Davis [37] recognize that the traditional vibration test methodology of controlling the interface environment at the test article only to a motion-based specification is often too conservative; inducing potentially excessive vibration responses at hardware resonant frequencies and a synopsis of the various remedial procedures proposed in the literature is presented. Of these, the dual-control or force-limited vibration test has recently emerged as a viable solution for ameliorating over test conditions on a wide variety of hardware. And discuss the practical implementation considerations in selecting the appropriate control variables**.** In addition Soucy and Cote [38] discuss the over testing problem associated with traditional vibration testing where the acceleration input to the base of a test article is controlled to specifications that are typically derived from the article interface acceleration at higher level of assembly . Some of the key features of the force limited vibration (FLV) testing are outlined. And the results of a collaborative effort between the Canadian Space Agency and Electro Mechanical Systems (EMS) in investigating and demonstrating the FLV testing by applying it to simple test articles are presented.

In an improved method Cote**,** et al. [39] give greater insights into the complex TDOFS method among the force-limited vibration methods, and propose methodologies to overcome its limitations. It is shown that a simple approach can be used to assure conservative estimate of the force limits in situations regarding closely spaced modes. It is also demonstrated that, although the complex TDOFS method is not perfectly adapted to fixed boundary conditions of the mounting structure, given certain precautions, it still provides good estimates of the force limits. And very recently, Soucy, et al. [40] present the main results and findings of a research and development project investigating the semi empirical method where the configuration-dependent constant parameter C is one of the key parameters of the method. More specifically, the project investigated the range of values taken by C (or C2) and the parameters on which it depends. They include the details and the results of an in-depth analytical sensitivity study of numerous cases and the results of the experimental validation of the analytical procedures.

Having seen nearly all the pertinent literatures it can be concluded that though a lot of research is being done on vibration testing based on motion or force responses, not much is done to use energy response as the criterion for notching. Thus this research is using as proposed a method of notching based on energy criterion in a limited spatial domain.

We next review from the literature some related research methodology used in vibration testing in addition to the concept and terminologies of impedance in Chapter 3. The concept further motivates the importance of new method as well as exhibit recent efforts and technology in eradication of over testing problem.

Chapter Three: Theoretical Basis

In this chapter we review some of the solution to the vibration over testing problem with their literature to provide the underlying theoretical support for the concern in this thesis. One of the main aim of this work shoots from a belief that we can ease the problem of over testing at resonances of the test item, which results from the standard practice of enveloping the peaks in the field acceleration spectral data, for both vibration and shock tests by taking into account the effect of impedance.

3.1 The Vibration Over Testing Problem

There are historically three solutions to the vibration over testing problem: 1) "build it like a brick", 2) mechanical impedance simulation, and 3) response limiting.

Some aerospace components are still "built like a brick" and therefore can survive vibration over testing and perhaps even an iterative test failure, rework, and retesting scenario. In a few cases, this may even be the cheapest way to go, but the frequency of such cases is certainly much less than it used to be. The two historical methods of alleviating over testing, impedance simulation and response limiting, are both closely related to force limiting.

3.1.1 Impedance Simulation

In the 1960's, personnel at NASA's Marshall Space Flight Center (MSFC) developed a mechanical impedance simulation technique called the "N plus one structure" concept, which involved incorporating a portion of the mounting structure into the vibration test. A common example would be the vibration test of an electronic board, mounted in a black box. In addition, acoustic tests were often conducted with the test items attached to a flight-like mounting structure. In all these approaches where a portion of the mounting structure, or simulated mounting structure, is used as the vibration test fixture, it is preferred that the acceleration input be specified and monitored internally at the interface between the mounting structure and the test item. If instead, the acceleration is specified externally at the interface between the shaker and mounting fixture, the impedance simulation benefit is greatly decreased. (When the input is defined internally, the "N plus one structure" approach is similar to the response limiting approach, discussed in the next section.)

A second example of mechanical impedance simulation is the multi-modal vibration test fixture scharton [11] which was designed to have many vibration modes to emulate a large flight mounting structure. This novel approach was used in one government program, a Mariner spacecraft, but fell by the wayside along with other mechanical impedance simulation approaches as being too specialized and too expensive. In addition, the concept went against the conventional wisdom of making fixtures as rigid as possible to avoid resonances.

Mechanical impedance simulation approaches are seldom employed because they require additional hardware and therefore added expense. Two exceptions which may find acceptance in this new low cost environment are: 1) deferring component testing until higher levels of assembly, e.g. the system test, when more of the mounting structure is automatically present, and 2) replacement of equipment random vibration tests with acoustic tests of the equipment mounted on a flight-like plate, e.g. honeycomb.

3.1.2 Response Limiting

Most institutions have in the past resorted to some form of response limiting as a means of alleviating vibration over testing. Response limiting is analogous to force limiting, but generally more complicated and dependent on analysis. Response limiting was used for several decades at JPL but has now been largely replaced by force limiting. In both response and force limiting, the approach is to predict the in flight response (force) at one or more critical locations on the item to be tested, and then to measure that response (force) in the vibration test and to reduce, or notch, the acceleration input in the test at particular frequencies, so as to keep the measured response (force) equal to or below that limit.

In the case of response limiting, the in-flight response is usually predicted with FEMs. This means that the prediction of response requires an FEM model of the test item and the directly excited supporting structure and the same model is typically used to design and analyze the loads in the test item. In this case the role of the test as an independent verification of the design and analysis is severely compromised. In addition, the model has to be very detailed in order to predict the in-flight response at critical locations, so the accuracy of the predictions is usually suspect, particularly at the higher frequencies of random vibration. By contrast, the

interface force between the support structure and test item can be predicted with more confidence, and depends less or not at all on the FEM of the test item.

In addition, it is often complicated or impossible to measure the responses at critical locations on the vibration test item. Sometimes the critical locations are not accessible, as in the case of optical and cold components. In the case of large test items, there may be many response locations of interest; hundreds of response locations may be measured in a typical spacecraft test. For this reason, some institutions rely completely on analysis to predict the responses in flight and in the test, and then a priori shape the input acceleration for the test in order to equate the flight and test responses. Since the uncertainty in the predictions of the resonance frequencies of the item on the shaker is typically 10 to 20 %, any notches based on pre-test analysis must be very wide, and may result in under testing at frequencies other than at resonances.

There is one form of response limiting which is conceptually identical to force limiting, i.e. limiting the acceleration of the center-of-gravity (CG) or mass centroid of the test item. By Newton's second law, the acceleration of the CG is equal to the external force applied to the body, divided by the total mass.

It is indeed much easier to predict the in flight responses of the test item CG, than the responses at other locations. The CG response is typically predicted with FEM's using only a lumped mass to represent the test item. At JPL a semi-empirical curve, called the mass-acceleration curve is usually developed early in the design process to predict the CG response of payloads. Also, any method used to predict the in-flight interface force obviously predicts the CG acceleration as well.

The problem with CG response limiting in the past has been that it is difficult or impossible to measure the acceleration of the CG with accelerometers in a vibration test. Sometimes the CG is inaccessible, or there is no physical structure at the CG location on which to mount an accelerometer. However, there is a more serious problem. The CG is only fixed relative to the structure, when the structure is a rigid body. Once resonances and deformations occur, it is impossible to measure the CG acceleration with an accelerometer. Furthermore attempts to measure the CG response usually overestimate the CG response at resonances, so limiting based on these measurements will result in an under test. However, the CG acceleration is

uniquely determined by dividing an interface force measurement by the total mass of the test item; this technique is very useful and will be discussed subsequently in conjunction with quasi-static design load verification.

3.1.3 Force Limiting

The purpose of force limiting is to reduce the response of the test item at its resonances on the shaker in order to replicate the response at the combined system resonances in the flight mounting configuration. Force limiting is most useful for structure-like test items which exhibit distinct, lightly damped resonances on the shaker. Examples are complete spacecraft, cantilevered structures like telescopes and antennas, lightly damped assemblies such as cold stages, fragile optical components, and equipment with pronounced fundamental modes such as a rigid structure with flexible feet.

There are virtually no flight data and little system test data on the vibratory forces at mounting structure and test item interfaces. Currently force limits for vibration tests are therefore derived using one of three methods: 1) calculated using two-degree-of freedom or other analytical models of the coupled source/load system together with measured or FEM effective mass data for the mounting structure and test item, 2) estimated using a semi-empirical method based on system test data and heuristic arguments, or 3) taken from the quasi-static design criteria which may be based on coupled loads analysis or a simple mass acceleration curve. In the first two methods, which are usually applicable in the random vibration frequency regime, the force specification is based on and proportional to the conventional acceleration specification. Any conservatism (or error) in the acceleration specification carries over to the force specification. In the third method, which is usually limited to static and low frequency sine-sweep or transient vibration tests, the force limit is derived independently from the acceleration specification.

3.1.4 Enveloping Tradition

The primary cause of vibration over testing is associated with the traditional, and necessary, practice of enveloping acceleration spectra to generate a vibration test specification. In the past the over testing, or conservatism as some preferred to call it, was typically attributed to the amount of margin that was used to envelope the spectral data or predictions. Now it is

understood that the major component of over testing is inherent in the enveloping process itself, and is not within the control of the person doing the enveloping.

In Figure 3.1, consider the data taken during the TOPEX spacecraft acoustic test Scharton [23]. Each of the six curves is a measurement near the attachment point of a different electronic box to a honeycomb panel. The flat trace is the test specification for the random vibration tests conducted on the electronic boxes, a year or so prior to the spacecraft acoustic test. Ideally the specification would just envelope the data, and the agreement is pretty good in the mid-frequency range from 100 to 500 Hz. One might rationalize that below 100 Hz, the random vibration specification is high to account for low frequency transients not simulated in the acoustic test, and above approximately 500 Hz the specification is high to account for direct acoustic excitation of the boxes which is not reflected in the attachment foot data. Therefore one may conclude that the random vibration test of the TOPEX spacecraft electronic boxes was not unduly conservative, but this would be erroneous. Each of the six curves in Fig. 3.1 has peaks and valleys, at different frequencies. The specification does a good job of enveloping all the peaks as it should, but what about the valleys. Clearly, the valleys are far below the specification, as illustrated by the dark highlighted curve. The next section, on the dynamic absorber effect, will show that that the frequencies associated with the valleys are very special, in that they represent the resonance frequencies of the boxes with fixed bases, i.e. as they are mounted in the random vibration tests on the shaker. In other words, the random vibration tests resulted in an over test at the box resonances, by the amount that the valleys in Fig. 3.1 are below the specification, i.e. typically 10 to 20 dB!

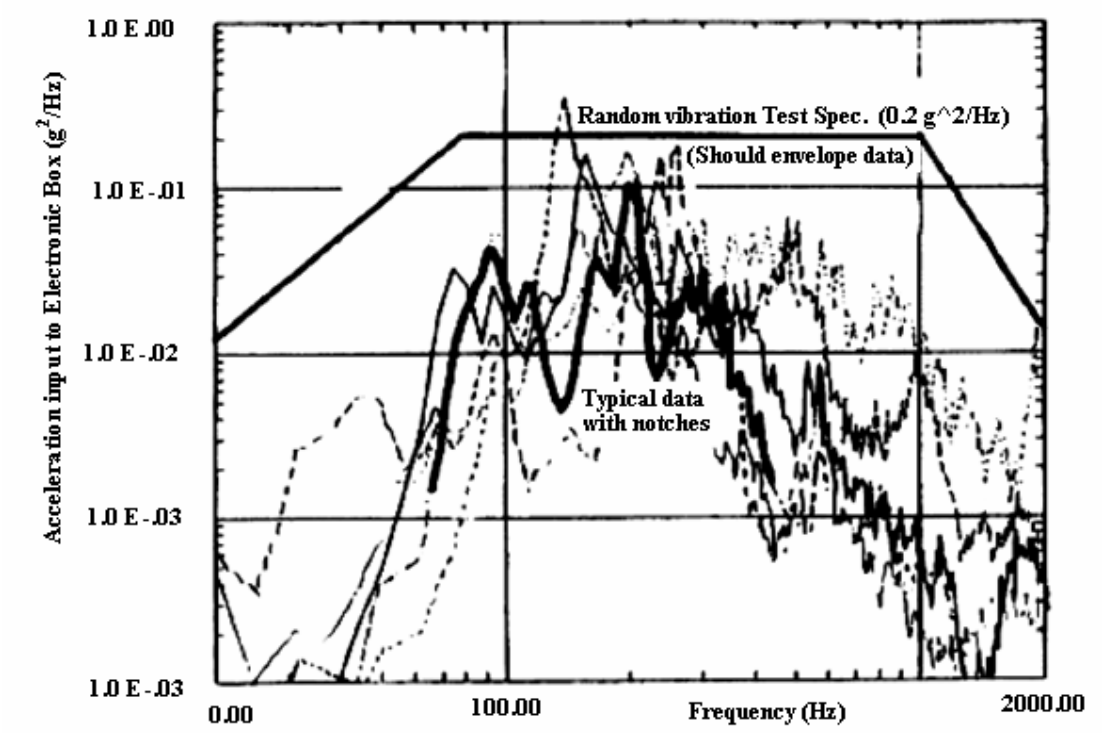

Figure 3-1 Measurements of Random Vibration Acceleration Spectra on Honeycomb Panel near Mounting Feet of Electronic Boxes in TOPEX Spacecraft Acoustic Test

Based on the preceding data, one might argue that random vibration specifications should envelope the valleys, not the peaks of the field data. However, this is not possible and would result in under testing off the resonances. The best approach, and the one implemented with force limiting, is to retain the traditional vibration test specification, which is the envelope of the peaks, but to notch the input at the resonance frequencies on the shaker to emulate the valleys in the field environment.

3.1.5 Dynamic Absorber Effect

The dynamic absorber effect scharton [41] may be explained with the assistance of Fig. 3.2, which shows a simple vibratory system consisting of two oscillators, connected in series. The primary oscillator is directly excited and the secondary oscillator is undamped and excited only by virtue of its connection to the first oscillator. The dynamic absorber effect refers to the fact that the motion of the mass of the primary, directly excited, oscillator will be zero at the natural frequency of the secondary oscillator. This statement is true even when the natural frequencies of the two oscillators are different and even when the mass of the secondary oscillator is much less than that of the secondary oscillator is small rather than zero, the motion of the primary mass is small rather than zero.

To apply the dynamic absorber effect to the aerospace vibration testing problem, assume that the two oscillator system in Fig. 3.2 represents a vibration mode of a flight support structure coupled to a vibration mode of a vibration test item. For example, the support structure might be a spacecraft, and the test item an instrument mounted on the spacecraft. Consider the numerical example illustrated in Fig. 3.3, for the case where the two uncoupled oscillator natural frequencies are identical, the masses are unity, the base acceleration is unity, and the Q is 50. The ordinates in Fig. 3.3 are FRF magnitudes, and for convenience the results are discussed in terms of a sinusoidal input. The abscissa in Fig. 3.3 is frequency, normalized by the natural frequency of an uncoupled oscillator. Fig. 3.3a is the magnitude of the coupled system interface force,

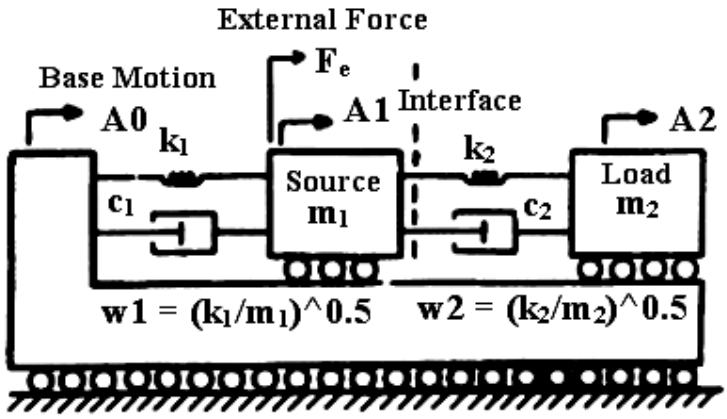

Figure 3-2 Simple Two-Degree-of-Freedom System (TDFS) directly excited oscillator. When the damping of the secondary oscillator is small rather than zero, the motion of the primary mass is small rather than zero.

Fig. 3.3b is the magnitude of the coupled system interface acceleration, and Fig. 3.3c is the magnitude of the load apparent mass. In Fig. 3.3, notice first that the interface force and interface acceleration both have peaks at the two coupled system resonance frequencies of 0.62 f_o and 1.62 f_o. Notice further that the interface acceleration has a notch of depth Q^{-1} at the load fixed-base resonance frequency f_o, where and the load apparent mass has a peak of height Q. This notch in the interface acceleration is just the dynamic absorber effect. This example illustrates the general dynamic absorber result, that the frequency spectrum of acceleration at the interface between the spacecraft and instrument will have notches at the fixed-base resonance frequencies of the instrument.

The example in Fig. 3.3 may also be used to illustrate the over testing resulting from enveloping the interface acceleration, and how force limiting will alleviate this over testing. In the coupled system, the interface force peak of 80 at the lower resonance frequency of 0.62 f_o results from multiplying the interface acceleration peak of 50 by the load apparent mass value of 1.6. In a conventional vibration test without force limiting, the corresponding shaker force would be of 2500, which is the interface acceleration envelope of 50 times the load apparent mass peak of 50 at the load resonance frequency f_o. With force limiting, the input acceleration would be notched at the load resonance frequency f_o to reduce the shaker force by a factor of 2500/80 or 31.25.

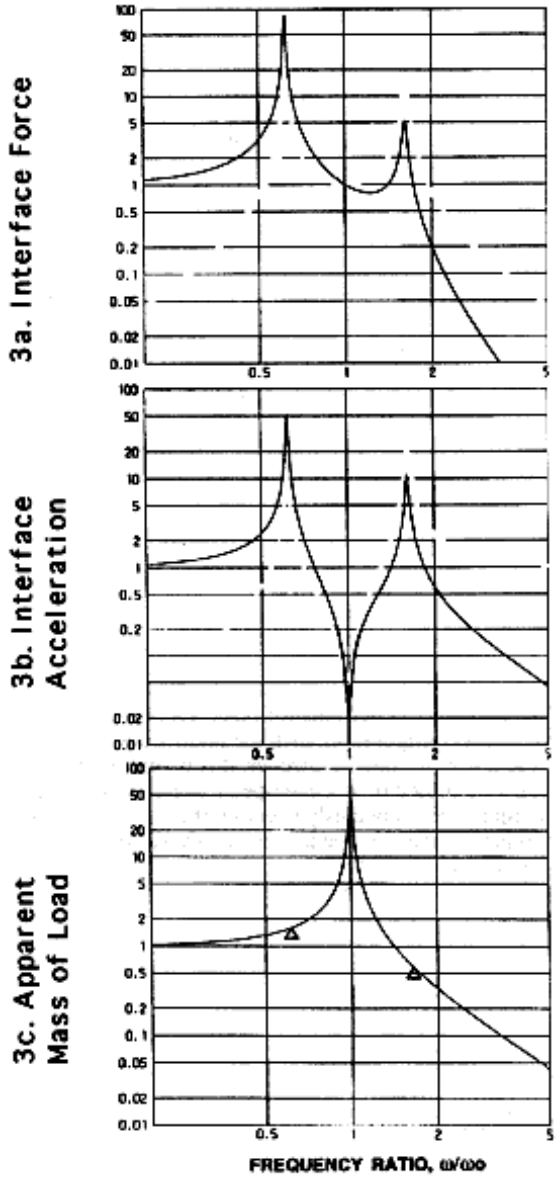

Figure 3-3 Interface Force, Interface Acceleration, and Load Apparent Mass FRF's for Simple TDFS in Figure 2.2 with $\omega_1 = \omega_2 = \omega_0$, $m_1 = m_2 = 1$, $A_0 = 1$ & $Q = 50$

3.2 Dual Control of Acceleration and Force

Conventional vibration tests are conducted by controlling only the acceleration input to the test item. In theory, if the frequency spectrum of the acceleration input in the test, including peaks and valleys, were identical to that of the interface acceleration in the flight mounting configuration, and if the boundary conditions for other degrees-of-freedom (rotations, etc.) were the same as in the flight configuration, then the interface forces and all the responses would be the same in the test as in flight. However, this is seldom the case, primarily because of the necessity of using a smoothed or an enveloped representation of the flight interface acceleration as the test input, and secondarily because of frequency shifts associated with the unrealistic restraint of other degrees-of-freedom by the shaker mounting. It has been found that the dual control of the acceleration and force input from the shaker alleviates the over testing problem associated with conventional vibration tests using only acceleration control.

3.2.1 Thevinen and Norton's Equivalent Circuit Theorems

Consider a source, consisting of a voltage source in series with a source impedance, which is connected to a load scharton [41]. If we adopt the mechanical analogy in which force is current and velocity is voltage, Thevinen's equivalent circuit theorem may be stated in mechanical terms as:

$$A = A_0 - F/M \qquad (3.1)$$

where A is the source-load interface acceleration, A_0 is the free acceleration (i.e., the acceleration that would exist at the interface if the load were removed), F is the interface force, and $\underline{M}$ is the source apparent mass measured at the interface. (Apparent mass is discussed in the next section.) All the terms in Equation 3.1 are complex and a function of frequency.

Using the same electo-mechanical analogy, consider a source, consisting of a current source in parallel with a source impedance, connected to a load. Norton's equivalent circuit theorem stated in mechanical terms is:

$$F = F_0 - AM \qquad (3.2)$$

where F_0 is the blocked force (i.e., the force that would be required at the interface to make the motion zero).

Equations Eqs. 3.1 and 3.2 may be manipulated to eliminate both F and A yielding the following relationship between the blocked force, free acceleration, and the source apparent mass:

$$F_0 / A0 = M \tag{3.3}$$

3.2.2 Dual Control Equations

Alternately, the source apparent mass M may be eliminated from Eq. 3.1 and Eq. 3.2, to yield the following Scharton and Kern [20]:

$$1 = A/A_0 + F/F_0, \tag{3.4}$$

which provides a theoretical basis for dual control of vibration tests.

Equation 3.4 is exact but difficult to apply because the terms on the right hand side are complex and complicated functions of frequency. The phase of the inputs and the impedance are difficult to determine analytically or experimentally, although some exploratory work on this problem was conducted some 25 years ago Ratz[5] and Hanter & Otts [14]. Little recent work on exact mechanical impedance simulation is available, and most commercially available vibration test controllers can not control phase angle to a specification.

An alternative, approximate formulation for the control of vibration tests is provided by the following extremal Eqs. Painter [11]:

$$|A|/|A_s|^2 \quad and \quad |F|/|F_s|^2 \ 1 \tag{3.5}$$

in which A_s represents the acceleration specification and F_s represents the force specification. In Eq. 3.5, the free acceleration and blocked force of Eq. 3.4 are replaced by the corresponding specifications which envelope the interface acceleration and force in the coupled system. With extremal control, the shaker current is adjusted in each narrow

frequency band so that the larger of the two ratios in Eq. 3.5 is equal to unity. At frequencies other than the test item resonances, the acceleration specification usually controls the test level; at the resonances, the base reaction force increases and the force specification limits the input.

Most vibration controllers have the capability for extremal control, but older controllers allow only one reference specification. To implement dual control in this case, a filter must be used to scale the shaker force feedback signal to an equivalent acceleration Judkins and Ranaudo [18]. New controllers allow separate specifications for limit channels, so Eq. 3.2 may be directly implemented. Force limiting has been used primarily for random vibration tests, but the application to swept sine tests is also practical and beneficial.

3.3 Structural Impedance Characterization

3.3.1 Apparent Mass

Structural impedance will be characterized as "apparent mass", which is the preferred name for the frequency response function (FRF) consisting of the ratio of reaction force to prescribed acceleration Scharton [41]. (Apparent mass symbols will be underscored in this paper to distinguish them from other mass quantities.) The force and prescribed acceleration in the apparent mass usually refer to the same degree-of-freedom. (In the literature, this is often called the "drive point" as distinguished from the "transfer" apparent mass.) The accelerations at other boundary degrees-of-freedom should be constrained to be zero if one is dealing with a multiple drive point problem O'Hara [3], but herein, only a single drive point is usually of interest, and this consideration is ignored. The apparent mass is generally a complex quantity, with magnitude and phase, but herein the term apparent mass will often be used in referring to only the magnitude.

The apparent mass can vary greatly with frequency, as one passes through resonances. Therefore the apparent mass reflects the stiffness and damping characteristics of a structure, as well as the mass characteristics.

The closed form solution for the apparent mass of a rod excited at one end and free at the other end is given by Scharton [41]:

$$\frac{F(\omega)}{A(\omega)} = M(\omega) = \left(\frac{i\rho_1 c}{\omega}\right)(1 + i\zeta) \qquad \frac{\tan(\pi\omega/2\omega_1) - i\tanh(\pi\zeta\omega/2\omega_1)}{1 + i\tan(\pi\omega/2\omega_1)\tanh(\pi\zeta\omega/2\omega_1)} \tag{3.6}$$

where: ρ_1 is the mass per unit length, c is the speed of longitudinal waves $(EA/\rho_1)^{1/2}$ where E is Young's modulus and A is cross-section area, ζ is the critical damping ratio, and w_1 is the fundamental frequency $\pi c/2L$ with L the rod length. This result is plotted as the solid line in Fig. 3.4 for a critical damping ratio ζ of 2.5%.

3.3.2 Effective Mass

Another mass-like quantity of great significance in structural analysis and for impedance simulation is the "effective mass" Wada et al. [15]. A formal definition of the effective mass, which encompasses multiple degrees-of-freedom and off-diagonal terms, as well as equations which enable the effective mass to be calculated, is given in the next section.

For the beam driven at one end, the apparent mass may also be expressed as a modal expansion involving the effective modal masses, m_n, and the single-degree-of-freedom frequency response factors:

$$M(\omega) = \sum_n m_n \frac{(1+i2\xi)}{\left\{\left|\left(1-(\omega/\omega_n)\right)^2\right| + i\xi\right\}}, \quad n=1,2,3,\ldots \tag{3.7}$$

where the structural form of damping has been assumed, M_o is the total mass ρ_l L, and m_n is the effective mass of the nth mode which is given by Scharton [41]:

$$m_n = 8M_0/[\pi^2(2n-1)^2] \tag{3.8}$$

where ω_n is the natural frequency of the nth mode which is equal to ω_1 (2n -1). Equation 3.7 may be viewed as a definition of the drive point effective mass. The sum of the effective masses over all the modes is the total mass, which may be verified by summing the rod effective masses, given by Eq. 3.8, over all n Scharton [41].

3.3.3 Residual Mass

Another mass quantity closely related to effective mass is the "residual mass", which is defined as the total mass minus the effective mass of the modes which have natural frequencies below the excitation frequency. Thus the residual mass of the Nth mode is:

$$M(N) = M_0 - \sum_{n=1 \text{ to } N} m_n \tag{3.9}$$

The residual mass may be interpreted as the fraction of the total mass which moves with the input acceleration, like a rigid body. A more precise definition of the residual mass concept, which encompasses multiple degrees-of-freedom and off-diagonal terms, is given in the next section.

It follows from the definition of residual mass, and the fact that the sum of the effective masses is the total mass, that the residual mass decreases monotonically to zero as frequency increases. This is the mechanical analogy of Foster's Theorem for electrical circuits Scharton [41]. Herein the residual mass is generally indicated with an upper case M. The effective modal mass is the negative change in the residual mass, at the resonance frequencies.

The effective modal and residual masses of the first five modes of the rod excited longitudinally are also shown in Fig. 3.4.

The dashed curve in Fig. 3.4 is the critically damped apparent mass which may be obtained from Eq. 3.6 by setting the critical damping ratio ζ equal to unity. The critically damped apparent mass is also called the "skeleton" function in electrical circuit analyses Scharton [41] or alternately the "infinite system" or "asymptotic" apparent mass.

The name "infinite system" derives from the second method of calculating this function which is by considering a semi-infinite system, e.g. the first factor on the right-hand-side of Eq. 3.6 Scharton [41]. Notice that the infinite system value of apparent mass of the rod decreases as one over frequency. This is also true for the apparent mass of a plate vibrating in bending.

The name asympotic derives from the third method of calculating this function which is to take a geometric average of the apparent mass FRF over frequency, so that there is equal area above and below the curve on a log-log plot Scharton [41]. (Observe the equal area characteristic of the critically damped apparent mass in Fig. 3.4.) The asymptotic form of the apparent mass is very important to the development herein, because it will be used to represent experimental apparent mass data measured either in tap tests or shaker tests. Notice in Fig. 3.4 that the asymptotic apparent mass is a generous envelope of the residual mass. The asymptotic apparent mass, which must include stiffness as well as mass contributions, is approximately equal to $2^{1/2}$ times the residual mass at the natural frequencies in Fig. 3.4. Herein the asymptotic apparent mass will be used as an approximation to the residual mass.

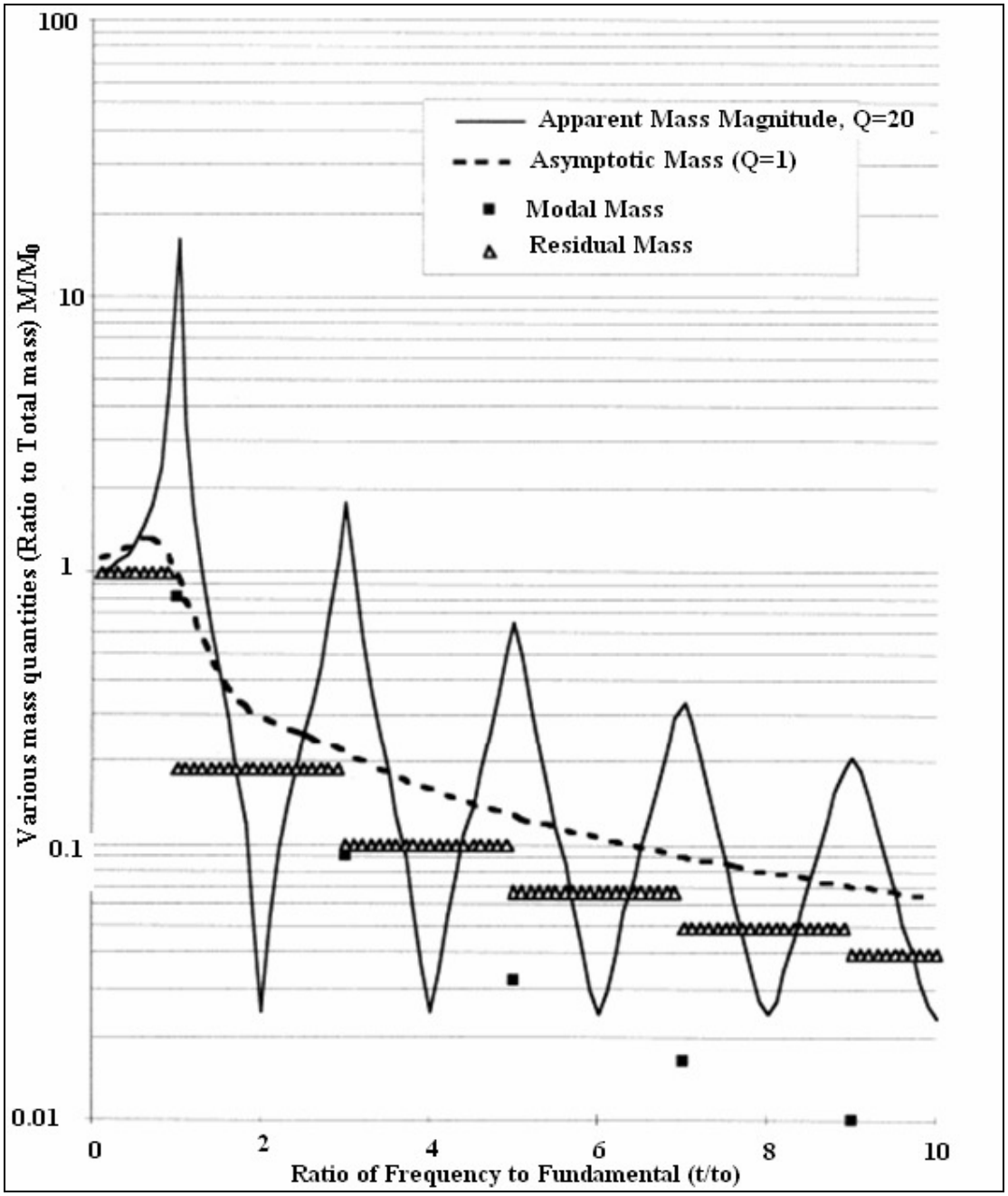

Figure 3-4 Apparent Mass, Asymptotic Mass, Modal Mass, and Residual Mass of Longitudinally Vibrating Rod, Excited at One End and Free at Other End

3.3.4 FEM Calculation of Effective Mass

Subdividing the displacement vector into unrestrained absolute displacements u_F and prescribed absolute displacements, u_P the equilibrium Equation is Wada et al. [15]:

$$\frac{[m_{FF}/m_{FP}]}{[m_{PF}/m_{PP}]}\left\{\frac{d^2u_F/dt^2}{d^2u_P/dt^2}\right\}+\frac{[k_{FF}/K_{FP}]}{[k_{PF}/K_{PP}]}\left\{\frac{u_F}{u_P}\right\}=\left\{\frac{f_F}{f_P}\right\} \tag{3.10}$$

Let: $$\{U\} = \emptyset U = \frac{[\emptyset_N/\emptyset_P]}{0/I_{PP}}\left\{\frac{U_N}{U_P}\right\} \quad (3.11)$$

where Φ_N are normal modes and Φ_R are rigid body modes associated with a kinematics set of unit prescribed motions, and U_N is the generalized modal relative displacement and U_P is the generalized prescribed absolute displacement. Substituting and pre-multiplying by Φ^T yields:

$$\frac{[M_{NN}/M_{NP}]}{[M^T{}_{NP}/M_{PP}]}\left\{\frac{d^2U_N/dt^2}{d^2U_P/dt^2}\right\} + \frac{[\omega^2{}_N M_{NN}/0]}{[0/0]}\left\{\frac{U_N}{U_P}\right\} = \left\{\frac{F_F}{F_P}\right\} \quad (3.12)$$

where: $$M_{NN} = \emptyset_N{}^T m_{FF} \emptyset_N \quad (3.13)$$

$$M_{NP} = \emptyset_N{}^T m_{FF} \emptyset_P + \emptyset_N{}^T m_{FP} I_{PP} \quad (3.14)$$

$$M_{PP} = I_{PP} m_{PP} I_{PP} + I_{PP} m_{PF} \emptyset_P + \emptyset_P{}^T m_{FP} I_{PP} + \emptyset_P{}^T m_{FF} \emptyset_P \quad (3.15)$$

$$F_P = I_{PP} f_P \quad (3.16)$$

For: $$d^2U_P/dt^2 = U_P = F_F = 0, d^2U_n/dt^2 = -\omega^2 U_n, and\ for\ U_n = 1$$

$$M_{NP}{}^T = -F_P/\omega_n{}^2, \quad (3.17)$$

where n indicates a single mode. (Note that $M_{nP}{}^T$ is in mass units.) M_{nP} is sometimes called the elastic-rigid coupling or the modal participation factor for the nth mode. If the model is restrained at a single point, the reaction (F_p) in Eq. 3.17 is the reaction force at that point in a modal analysis.

The initial value of M_{PP} is the rigid body mass matrix. If a Gaussian decomposition of the total modal mass in Eq. 3.12 is performed, it subtracts the contribution of each normal mode, called the effective mass:

$$M_{np}{}^T M_{nn}{}^T M_{np} \quad (3.18)$$

from the current M_{PP}^{n}, which is the residual mass after excluding the mass associated with the already processed n modes.

Consider the ratio of the reaction force in a particular direction p, to the prescribed acceleration in a particular direction q; the effective mass, $M_{np}^{T} M_{nn}^{-1} M_{nq}$, is the same as the contribution of the nth mode to this ratio, divided by the single-degree-of-freedom frequency response factor. Please note that the values of the effective mass are independent of the modal normalization.

Generally the reaction is desired in the same direction as the excitation and the effective mass for the common direction is a diagonal of the $M_{nP}^{T} M_{nn}^{-1} M_{nP}$ 6x6 matrix, and the residual mass for that element monotonically decreases as more and more modes are processed. The sum of the common-direction effective masses for all modes is equal to the total mass, or moment of inertia for that direction. If there is no common direction, the foregoing is not true. If $m_{FP} = m_{PP}=0$ the residual mass after processing a complete set of modes is a 6x6 null matrix. If m_{FP} and m_{PP} are not equal to zero, the value of M_{PP}^{N} after processing a complete set of modes is: $m_{PP} - m_{FP}^{T} \Phi_N M_{NN}^{-1} \Phi_N^{T} m_{FP}$, which must be positive definite.

The highest reaction of a single mode for a given excitation level may not occur along one of the axes used in analysis or test. The highest reaction force (not moment) will occur for excitation along an axis such that its direction cosines are proportional to the diagonal terms of the effective mass along the analysis axis. The effective mass along this axis is $(M_{1n}^{2}+M_{2n}^{2}+M_{3n}^{2}) / M_{nn}$.

All of the concepts of impedance reviewed in this chapter collectively contribute to the reduction of over testing problem. In the next chapter (Chapter 4) we go through a detailed mathematical modeling of response spectrum for the dynamic analysis of the structure on ANSYS applied for the satellite which is going to be model.

Chapter Four: Mathematical Formulation of the Problem

4.1 Dynamic Analysis

The dynamic analysis is the analysis of the system under consideration when forces are acting on the system. It considers external excitation forces and inertia forces. FEM approach is widely used to solve dynamic analysis problems. The dynamic analysis is divided into two types either transient or response spectrum. In case of transient response the forcing functions are defined as functions of time. While in response spectrum they are functions of frequency. In the project it uses spectrum response analysis and it is discussed in this section.

4.2 Analysis of Response Spectrum

A response spectrum is simply a plot of the peak or steady-state response (displacement, velocity or acceleration) of a series of oscillators of varying natural frequency that are forced into motion by the same base vibration or shock. The resulting plot can then be used to pick off the response of any linear system, given its natural frequency of oscillation. One such use is in assessing the peak response of structures to seismic loads.

Response spectrum can also be used in assessing the response of linear systems with either direct or modal frequency response (multi-degree of freedom systems), although they are only accurate for low levels of damping.

The main limitation of response spectra is that they are only universally applicable for linear systems. Response spectra can be generated for non-linear systems, but are only applicable to systems with the same non-linearity, although attempts have been made to develop non-linear seismic design spectra with wider structural application. It should be noted that the results cannot be directly combined for multi-mode response.

4.3 Analysis of Dynamic Response Using Superposition

4.3.1 Normal Coordinates

In the preceding discussion of an arbitrary N-DOF linear system, the displaced position was defined by the N components in the vector **v**. However, for the purpose of dynamic response analysis, it is often advantageous to express this position in terms of the free-vibration mode shapes. These shapes constitute N independent displacement patterns, the amplitudes of

which may serve as generalized coordinates to express any set of displacements. The mode-shapes thus serve the same purpose as the trigonometric functions in a Fourier series, and they are used for the same reasons; because: (1) they possess orthogonality properties and (2) they are efficient in the sense that they usually can describe all N displacements with sufficient accuracy employing only a few shapes.

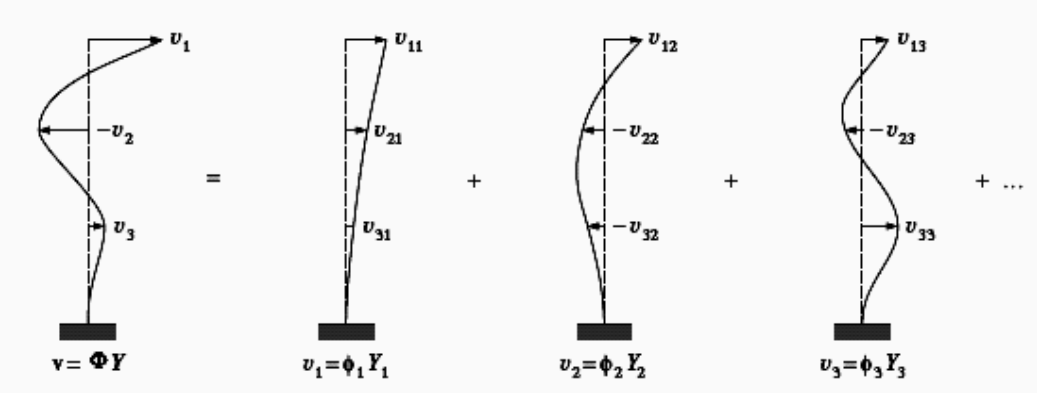

Figure 4-1 Representing Deflections as Sum of Modal Components

Consider, for example, the cantilever column shown in Fig. 4.1, for which the deflected shape is expressed in terms of translational displacements at three levels. Any displacement vector **v** (static or dynamic) for this structure can be developed by superposing suitable amplitudes of the normal modes as shown. For any modal component $\mathbf{v}_n$, the displacements are given by the product of the mode shape vector Φ_n and the modal amplitude Y_n; thus

$$v_n = \emptyset_n Y_n \tag{4.1}$$

The total displacement vector **v** is then obtained by summing the modal vectors as expressed by

$$v = \emptyset_1 Y_1 + \emptyset_2 Y_2 + \cdots + \emptyset_N Y_N = \sum_{n=1}^{N} \emptyset_n Y_n \tag{4.2}$$

or, in matrix notation,

$$v = \emptyset Y \tag{4.3}$$

In this equation, it is apparent that the N X N mode-shape matrix Φ serves to transform the generalized coordinate vector $\boldsymbol{Y}$ to the geometric coordinate vector **v**. The generalized components in vector $\boldsymbol{Y}$ are called the normal coordinates of the structure.

Because the mode-shape matrix consists of N independent modal vectors, $\boldsymbol{\Phi} = [\boldsymbol{\phi}_1 \ \ \boldsymbol{\phi}_2 \ \cdots \ \boldsymbol{\phi}_N]$, it is nonsingular and can be inverted. Thus, it is always possible to solve Eq. (4.3) directly for the normal-coordinate amplitudes in $\boldsymbol{Y}$ which are associated with any given displacement vector **v**. In doing so, however, it is unnecessary to solve a set of simultaneous equations, due to the orthogonality property of the mode shapes. To evaluate any arbitrary normal coordinate, Y_n for example, premultiply Eq. (4.2) by $\emptyset_n^T m$ to obtain

$$\emptyset_n{}^T mv = \emptyset_n^T m\emptyset_1 Y_1 + \emptyset_n^T m\emptyset_2 Y_2 + \cdots + \emptyset_n^T m\emptyset_N Y_N \tag{4.4}$$

Because of the orthogonality property with respect to mass, i.e., $\emptyset_n^T m\emptyset_m = 0$ for m ≠ n, all terms on the right hand side of this equation vanish, except for the term containing $\emptyset_n^T m\emptyset_N$, leaving

$$\emptyset_n^T mv = \emptyset_n^T m\emptyset_n Y_n \tag{4.5}$$

from which

$$Y_N = \frac{\emptyset_n^T mv}{\emptyset_n^T m\emptyset_n} \qquad\qquad n = 1, 2, \ldots, N \tag{4.6}$$

If vector **v** is time dependent, the Y_n coordinates will also be time dependent; in this case, taking the time derivative of Eq. (4.6) yields

$$\dot{Y}_n(t) = \frac{\emptyset_n^T m\dot{v}(t)}{\emptyset_n^T m\emptyset_n} \tag{4.7}$$

Note that the above procedure is equivalent to that used to evaluate the coefficients in the Fourier series.

4.3.2 Uncoupled Equations of Motion: Undamped

The orthogonality properties of the normal modes will now be used to simplify the equations of motion of the MDOF system. In general form these equations are given by, for the undamped system it become

$$m\ddot{v}(t) + kv(t) = p(t) \tag{4.8}$$

Introducing Eq. (4.3) and its second time derivative $\mathbf{v} = \boldsymbol{\Phi}\,\mathbf{Y}$ (noting that the mode shapes do not change with time) leads to

$$m\emptyset\ddot{Y}(t) + k\emptyset Y(t) = p(t) \tag{4.9}$$

If Eq. (4.9) is premultiplied by the transpose of the nth mode-shape vector Φ^{T}, it becomes

$$\emptyset_n^T m\emptyset\ddot{Y}(t) + \emptyset_n^T k\emptyset Y(t) = \emptyset_n^T p(t) \tag{4.10}$$

but if the two terms on the left hand side are expanded as shown in Eq. (4.4), all terms except the nth will vanish because of the mode-shape orthogonality properties; hence the result is

$$\emptyset_n^T m\emptyset_n\ddot{Y}(t) + \emptyset_n^T k\emptyset_n Y(t) = \emptyset_n^T p(t) \tag{4.11}$$

Now new symbols will be defined as follows:

$$M_n \equiv \emptyset_n^T m\emptyset_n \tag{4.12a}$$

$$K_n \equiv \emptyset_n^T k\emptyset_n \tag{4.12b}$$

$$P_n \equiv \emptyset_n^T p(t) \tag{4.12c}$$

which are called the normal-coordinate generalized mass, generalized stiffness, and generalized load for mode n, respectively. With them Eq. (4.11) can be written

$$M_n Y_n(t) + K_n Y_n(t) = P(t) \tag{4.13}$$

which is a SDOF equation of motion for mode n. If the equation $\mathbf{k}\Phi n = \omega^2_n \mathbf{m}\Phi_n$, is multiplied on both sides by $\emptyset_n^T$, the generalized stiffness for mode n is related to the generalized mass by the frequency of vibration

$$\emptyset_n{}^T k \emptyset_n = \omega_n^2 \emptyset_n^T m \emptyset_n$$

or
$$K_n = \omega_n^2 M_n \tag{4.12d}$$

(Capital letters are used to denote all normal-coordinate properties.)

The procedure described above can be used to obtain an independent SDOF equation for each mode of vibration of the undamped structure. Thus the use of the normal coordinates serves to transform the equations of motion from a set of N simultaneous differential equations, which are coupled by the off-diagonal terms in the mass and stiffness matrices, to a set of N independent normal-coordinate equations. The dynamic response therefore can be obtained by solving separately for the response of each normal (modal) coordinate and then superposing these by Eq. (4.3) to obtain the response in the original geometric coordinates. This procedure is called the *mode-superposition method*, or more precisely the *mode displacement superposition method*.

4.3.3 Uncoupled Equations of Motion: Viscous Damping

Now it is of interest to examine the conditions under which this normal-coordinate transformation will also serve to uncouple the damped equations of motion. These equations are

$$m\ddot{v}(t) + c\dot{v}(t) + kv(t) = p(t)$$

Introducing the normal-coordinate expression of Eq. (4.3) and its time derivatives and premultiplying by the transpose of the nth mode-shape vector $\emptyset_n^T$ leads to

$$\emptyset_n{}^T m\emptyset\ddot{Y}(t) + \emptyset_n{}^T c\emptyset\dot{Y}(t) + \emptyset_n{}^T k\emptyset Y(t) = \emptyset_n{}^T p(t) \tag{4.14}$$

It was noted above that the orthogonality conditions

$$\emptyset_n^T m\emptyset_n = 0$$

$$m \neq n$$

$$\emptyset_n^T k\emptyset_n = 0$$

cause all components except the nth-mode term in the mass and stiffness expressions of Eq. (4.14) to vanish. A similar reduction will apply to the damping expression if it is assumed that the corresponding orthogonality condition applies to the damping matrix; that is, assume that

$$\emptyset_n^T m\emptyset_n = 0 \qquad m \neq n \tag{4.15}$$

In this case Eq. (4.14) may be written

$$M_n\ddot{Y}_n(t) + C_n\dot{Y}_n(t) + K_nY_n(t) = P(t) \tag{4.14a}$$

where the definitions of modal coordinate mass, stiffness, and load have been introduced from Eq. (4.12) and where the modal coordinate viscous damping coefficient has been defined similarly

$$C_n \equiv \emptyset_n^T c \emptyset_n \tag{4.15a}$$

If Eq. (4.14a) is divided by the generalized mass, this modal equation of motion maybe expressed in alternative form:

$$\ddot{Y}_n(t) + 2\xi_n \omega_n \dot{Y}_n(t) + \omega_n^2 Y_n(t) = \frac{P(t)}{M_n} \tag{4.14b}$$

where Eq. (4.12d) has been used to rewrite the stiffness term and where the second term on the left hand side represents a definition of the modal viscous damping ratio

$$\xi_n = \frac{C_n}{2\omega_n M_n} \tag{4.15b}$$

As was noted earlier, it generally is more convenient and physically reasonable to define the damping of a MDOF system using the damping ratio for each mode in this way rather than to evaluate the coefficients of the damping matrix **c** because the modal damping ratios ξ_n can be determined experimentally or estimated with adequate precision in many cases.

4.4 Response Analysis for Time and Frequency Domain

Viscous Damping

The normal coordinate transformation was used in Section 4.3 to convert the N coupled linear damped equations of motion

$$m\ddot{v}(t) + c\dot{v}(t) + kv(t) = p(t) \tag{4.16}$$

to a set of N uncoupled equations given by

$$\ddot{Y}_n(t) + 2\xi_n \omega_n \dot{Y}_n(t) + \omega_n^2 Y_n(t) = \frac{P(t)}{M_n} \qquad n = 1,2,\dots,N \tag{4.17}$$

in which

$$M_n = \emptyset_n^T m \emptyset_n \qquad P_n = \emptyset_n^T p(t) \tag{4.18}$$

To proceed with the solution of these uncoupled equations of motion, one must first solve the eigenvalue problem

$$[k - \omega^2 m]\, \hat{v} = 0 \tag{4.19}$$

to obtain the required mode shapes Φ_n (n = 1, 2, **…**) and corresponding frequencies ω_n. The modal damping ratios ξ_n are usually assumed based on experimental evidence.

The total response of the MDOF system now can be obtained by solving the N uncoupled modal equations and superposing their effects, as indicated by Eq. (4.3). Each of Eqs. (4.17) is a standard SDOF equation of motion and can be solved in either the time domain or the frequency domain. The time-domain solution is expressed by the Duhamel integral

$$Y_n(t) = \frac{1}{M_n \omega_{D_n}} \int_0^t P_n(\tau) exp[-\xi_n \omega_n (t-\tau)] \sin \omega_{D_n} (t-\tau) d\tau \tag{4.20}$$

which also may be written in standard convolution integral form

$$Y_n(t) = \int_0^t P_n(\tau) h_n(t-\tau) d\tau \tag{4.21}$$

in which

$$h_n(t-\tau) = \frac{1}{M_n \omega_{Dn}} \sin \omega_{Dn}(t-\tau) exp[-\xi_n \omega_n (t-\tau)] \;\; 0 < \xi_n < 1 \qquad (4.22)$$

is the unit-impulse response function.

In the frequency domain, the response is obtained from

$$Y_n(t) = \frac{1}{2\pi} \int_{-\infty}^{\infty} H_n(i\bar{\omega}) \;\; P(i\bar{\omega}) \; exp i\bar{\omega} t \; d\bar{\omega} \qquad (4.23)$$

In this equation, the complex load function $P_n(i\omega)$ is the Fourier transform of the modal loading $P_n(t)$ is given by

$$P(i\bar{\omega}) = \int_{-\infty}^{\infty} P_n(t) \;\; exp(-i\bar{\omega} t) \; dt \qquad (4.24)$$

Also in Eq. (4.23), the complex frequency response function, $H_n(i\bar{\omega})$, may be expressed as follows:

$$H_n(i\bar{\omega}) = \frac{1}{\omega_n^2 M_n} \left[\frac{1}{(1-\beta_n^2) + i(2\xi_n \beta_n)} \right]$$

$$= \frac{1}{\omega_n^2 M_n} \left[\frac{1}{(1-\beta_n^2) + i(2\xi_n \beta_n)} \right] \qquad \xi_n \geq 0 \qquad (4.25)$$

In these functions, $\beta_n \equiv \bar{\omega}/\omega_n$ and $\omega_{Dn} = \omega_n \sqrt{1-\xi_n^2}$. $h_n(t)$ and $H_n(i\bar{\omega})$ are Fourier transform pairs. Solving Eq. (4.20) or (4.23) for any general modal loading yields the modal response $Y_n(t)$ for $t \geq 0$, assuming zero initial conditions, i.e., $Y_n(0) = \dot{Y}_n(0) = 0$. Should the initial conditions not equal zero, the damped free-vibration response

$$Y_n(t) = \left[Y_n(0) \;\; cos \, \omega_{Dn} t + \left(\frac{\dot{Y}_n(0) + Y_n(0) \xi_n \omega_n}{\omega_{Dn}} \right) \; sin \, \omega_{Dn} t \right] exp(-\xi_n \omega_n t) \qquad (4.26)$$

must be added to the forced-vibration response given by Eqs. (4.20) or (4.23). The initial conditions $Y_n(0)$ and $\dot{Y}_n(0)$ in this equation are determined from $\mathbf{v}(0)$ and $\dot{\mathbf{v}}(0)$ using Eqs. (4.6) and (4.7) in the forms

$$Y_N(0) = \frac{\phi_n^T m v(0)}{\phi_n^T m \phi_n} \tag{4.27}$$

$$\dot{Y}_n(0) = \frac{\phi_n^T m \dot{v}(0)}{\phi_n^T m \phi_n} \tag{4.28}$$

Having generated the total response for each mode $Y_n(t)$ using either Eq. (4.20) or Eq. (4.23) and Eq. (4.26), the displacements expressed in the geometric coordinates can be obtained using Eq. (4.2), i.e.,

$$v(t) = \phi_1 Y_1(t) + \phi_2 Y_2(t) + \cdots + \phi_N Y_N(t) \tag{4.29}$$

which superposes the separate modal displacement contributions; hence, the commonly referred to name mode superposition method. It should be noted that for most types of loadings the displacement contributions generally are greatest for the lower modes and tend to decrease for the higher modes. Consequently, it usually is not necessary to include all the higher modes of vibration in the superposition process; the series can be truncated when the response has been obtained to any desired degree of accuracy. Moreover, it should be kept in mind that the mathematical idealization of any complex structural system also tends to be less reliable in predicting the higher modes of vibration; for this reason, too, it is well to limit the number of modes considered in a dynamic-response analysis.

The displacement time-histories in vector v(t) may be considered to be the basic measure of a structure's overall response to dynamic loading. In general, other response parameters such as stresses or forces developed in various structural components can be evaluated directly from the displacements. For example, the elastic forces $\mathbf{f}_S$ which resist the deformation of the structure are given directly by

$$f_s(t) = kv(t) = k\emptyset Y(t) \tag{4.30}$$

An alternative expression for the elastic forces may be useful in cases where the frequencies and mode shapes have been determined from the flexibility form of the eigenvalue equation. Writing Eq. (4.30) in terms of the modal contributions

$$f_s(t) = k\emptyset_1 Y_1(t) + k\emptyset_2 Y_2(t) + k\emptyset_3 Y_3(t) + \cdots \tag{4.31}$$

leads to

$$f_s(t) = \omega_1^2 m\emptyset_1 Y_1(t) + \omega_2^2 k\emptyset_2 Y_2(t) + \omega_3^3 m\emptyset_3 Y_3(t) + \cdots \tag{4.32}$$

Writing this series in matrix form gives

$$f_s(t) = m\emptyset\{\omega_n^2 Y_n(t)\} \tag{4.33}$$

where $\{\omega^2_n\ Y_n(t)\}$ represents a vector of modal amplitudes each multiplied by the square of its modal frequency.

In Eq. (4.33), the elastic force associated with each modal component has been replaced by an equivalent modal inertial-force expression. The equivalence of these expressions was demonstrated from the equations of free-vibration equilibrium; however, it should be noted that this substitution is valid at any time, even for a static analysis.

Because each modal contribution is multiplied by the square of the modal frequency in Eq. (4.33), it is evident that the higher modes are of greater significance in defining the forces in the structure than they are in the displacements. Consequently, it will be necessary to include

more modal components to define the forces to any desired degree of accuracy than to define the displacements.

4.5 Mode Combination

Modal analysis is performed to identify the modes, and the response in that mode can be picked from the response spectrum. This peak response is then combined to estimate a total response. A typical combination method is the square root of the sum of the squares (SRSS) if the modal frequencies are not close.

The displacement, velocity or acceleration vector for each mode is computed from the eigenvector by using a "mode coefficient":

$$\{r_i\} = \omega_i{}^m A_i \{\emptyset\}_i \tag{4.16}$$

where: m = 0, 1, or 2, based on whether the displacements, velocities, or accelerations, respectively, are selected.

Ai = mode coefficient

The mode coefficient is computed for acceleration excitation of base

$$A_i = \frac{S_{ai} \gamma_i}{\omega_i{}^2} \tag{4.17}$$

where: S_{ai} = spectral acceleration for the ith mode (obtained from the input acceleration response spectrum at frequency f_i and effective damping ratio

γ_i = participation factor for the ith mode.

The participation factors for a given excitation directions are defined as:

$$\gamma_i = \{\emptyset\}_i^T [M]\{D\} \tag{4.18}$$

where: γ_i = participation factor for the ith mode

{D} = vector describing the excitation direction

The modal displacements, velocity and acceleration (Equation 4.16) may be combined in different ways to obtain the response of the structure. The response includes DOF response as well as element results and reaction forces.

Only those modes having significant amplitude (mode coefficient) are chosen for mode combination. A mode having a coefficient of greater than a given value of the maximum mode coefficient (all modes are scanned) is considered significant.

The combination is done by a generalization of the method of the square root of the sum of the squares which has the form:

$$R_a = \left[\sum_{i=1}^{N}\sum_{j=1}^{N} \varepsilon_{ij} R_i R_j\right]^{1/2} \tag{4.19}$$

where:

R_a = total modal response

N = total number of expanded modes

ε_{ij}= coupling coefficient. The value of ε_{ij} = 0.0 implies modes i and j are independent and approaches 1.0 as the dependency increases

$R_i = A_i\Psi_i$ = modal response in the i^{th} mode (Equation 4.16)

$R_j = A_j\Psi_j$ = modal response in the j^{th} mode

A_i = mode coefficient for the i^{th} mode

A_j = mode coefficient for the j^{th} mode

Ψ_i = the i^{th} mode shape

Ψ_j = the j^{th} mode shape

Ψi and Ψj may be the DOF response, reactions, or stresses. The DOF response, reactions, or stresses may be displacement, velocity or acceleration.

For the case of the SRSS (Square Root of the Sum of the Squares) Method, Equation (4.19) reduces to:

$$R_a = \left[\sum_{i=1}^{N} R_i^{\,2}\right]^{1/2} \tag{4.19}$$

Having seen the theory of mathematical modeling of a structure for spectrum analysis in the next chapter (Chapter Five) we go through the detail of the modeling of the satellite with the review of design of satellite strictures from literatures.

Chapter Five: FE Modeling and Analysis of a Satellite Structure

To get a good understanding and practical experience with the energy limiting method, a simple satellite structure is modeled, and analyzed. Therefore this section describes the FE modeling and analysis of a satellite that is devised as a multipurpose bus for scientific application with the introduction part including the collected information from the literature to meet the modeling of the satellite.

The modeled structure includes a main body (platform & frame), an adapter, two solar panels and some instruments that controlled and communicated the satellite. It is overall shape resembles a hexagonal prism weighting about 1030Kg. The configuration of the satellite is 500 mm in major diameter, and approximately 1050 mm in height. The platforms are assumed consists of aluminium frames and connected by means of welding. The mission loads (payloads) are assembled on the top of the honeycomb platforms. The analysis of the structure is divided into two parts: static and dynamic properties. The static analysis ensures that the structure can withstand axial inertial g load and support the masses of the payloads during launch, and the dynamic analysis investigates the stiffness properties and prediction of notching of the structure for test attachment.

5.1 Introduction

5.1.1 Satellite's Missions

Satellites provide numerous services for modern society. They perform essential duties for military, governmental, and commercial organizations. The missions of these spacecraft include science ventures such as earth observation, interplanetary exploration, astronomy, and solar physics. They also include commercial endeavours such as television signal transmission, data transmission, and satellite telephone communication.

The majority of the space science missions are performed by NASA-built spacecraft. The design and size of these spacecraft are highly dependent on the mission goals. These goals are constantly evolving due to changes in technology, political agenda, and budget. As a result, the design and size of satellites reflect these changes. This phenomenon is readily proven by examining the masses of civilian spacecraft launched throughout history. Figure 5.1 displays the launch mass of several NASA spacecraft as a function of time. The plot shows a gradual mass increase until the early 1990s at which point the spacecraft masses suddenly begin to

decrease. This sharp decrease is primarily due to the change in policies at NASA towards the “faster, better, cheaper" program and a decrease in the overall NASA budget. These smaller spacecraft are inherently less expensive to launch. The subsystems can therefore afford to take a high risk/low cost approach toward the design and offer less redundancy. This decrease in redundancy also decreases the overall cost and size of the spacecraft. NASA is now using constellations or formations of small-satellite systems to perform missions that once required large multi-million dollar spacecraft.

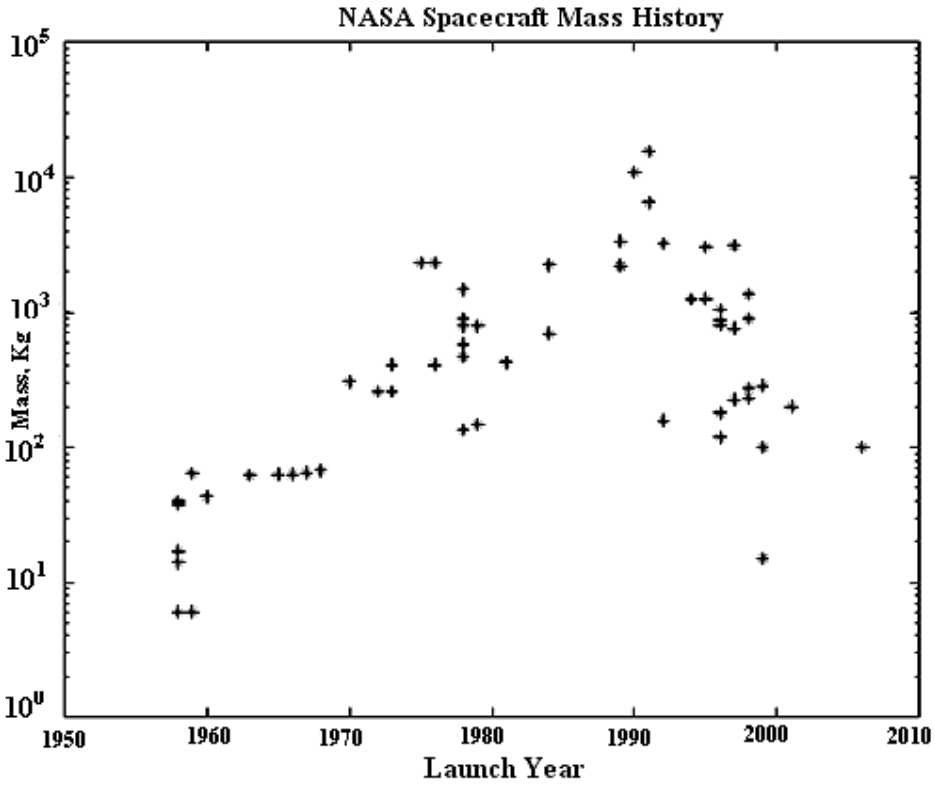

Figure 5-1 Launch Mass History of NASA Spacecraft

The commercial spacecraft industry has also evolved throughout history, as shown in Figure 5.2. However, the masses have not decreased as significantly due to several factors. A major factor for this trend is the high gain antennas and large power requirements inherent to the communications satellites placed in geosynchronous orbit. The communications industry has long exploited the phenomena of “fixed" geosynchronous spacecraft to provide a stationary signal to its ground-based antennas. This current practice appears to be changing, however, as distributed spacecraft systems become more prevalent (eg: XM radio, Globalstar, etc.).

As we have shown, the satellite industry has transformed to match the ever-changing environment of technology. Spacecraft mass, as a result, has also demonstrated this trend.

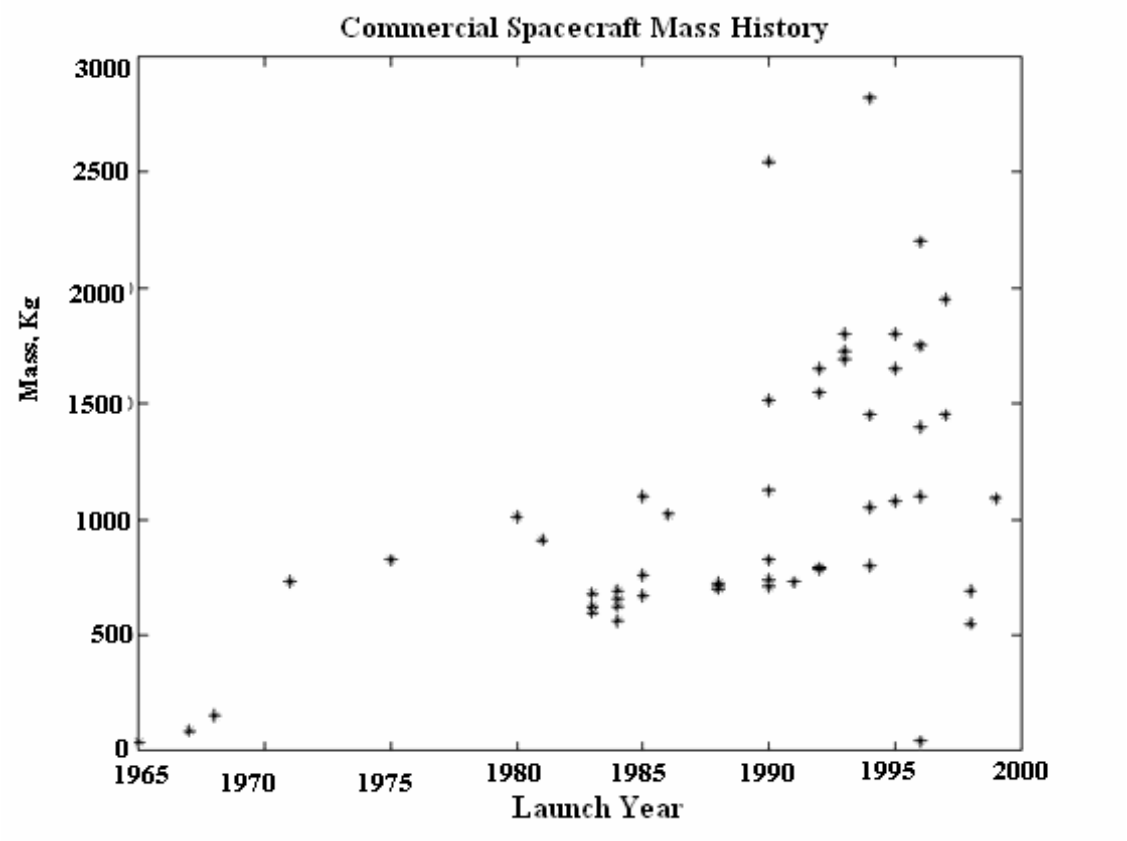

Figure 5-2 Launch Mass History of Commercial Spacecraft

5.1.2 Satellite Structures

Aerospace structures generally require lightweight designs. The goal of these designs is to optimize the strength per weight, or efficiency of the design. Satellite structural design has evolved greatly over the past four decades. Traditionally, efficiency has been accomplished using a combination of various structural designs and materials. We begin this section by discussing basic primary structural designs and conclude by presenting traditional materials used in spacecraft.

5.1.2.1 Conventional Structural Designs

Primary structures are designed using several criteria that depend on the mission requirements. Conventional spacecraft incorporate four basic primary structural designs: 1) skin-frame structures; 2) truss structures; 3) monocoque cylinders; and 4) skin-stringer structures.

The skin-frame structural design uses an interior skeletal network of axial and lateral frames to mount exterior skin panels using fasteners or rivets. The frames support bending, torsional, and axial forces. The skin reinforces the structure by supporting the shear forces introduced by the interior member connections. The skin is sometimes minimized to save mass, even though the thin skin leads to some structural instabilities. When the skin buckles due to shear, it transfers all additional shear loading to in-plane tension forces at 45^{o} which must be supported by the connections. The buckling modes of the skin exhibit large deformations that make it insufficient for exterior mounted components such as solar cells. The buckling strength of the assembly is typically increased by adding intermediate members.

Truss structures use an array of members that can only support axial loads. Truss members are produced independently and arranged typically in arrays of triangles for stability. The members are manufactured using extruded tubes made of composite, metallic, or sheet metal materials. A stable truss is statically determinate and has no excess members to introduce alternate load paths. Trusses are generally mass-efficient when the members are configured into rectangular or triangular cross-sectional assemblies. However, they become less efficient as the cross-section becomes more circular or hexagonal. Also, the design of the structure creates inherent stress concentrations at interface mounting points, such as separation systems. Components may be mounted both internally and externally and the absence of shear panels enables easy access to a payload. However, this absence of shear panels is not helpful to spacecraft requiring body mounted solar cells.

Monocoque cylinders are axisymmetric shells that do not contain any stiffeners or frames. The shells are manufactured using metallic or sandwich panels with curved sections formed by rolling. Typically, two or three curved sections are fabricated and assembled into the cylindrical configuration. The strength of monocoque cylinders is usually limited by its buckling strength. The shells are most efficient when the loads are distributed evenly throughout the structure. Components are typically mounted to the walls using fasteners; however, care must be taken not to overload the shell and cause local failures. The monocoque cylinder design is applicable to spacecraft with body mounted solar cells and relatively lightweight components.

Cylindrical skin-stringer structures are designed using axial and lateral frame members attached to an outer skin. These designs are similar to skin-frame structures; however, this

class of structures refers to circular cylinder configurations. The skin is sometimes minimized to save mass, even though the thin skin leads to some structural instabilities. The post-buckling behaviour of the skin transfers the additionally applied shear loads to torsion by the diagonal tension phenomenon described above. The skin and members must attach uniformly to enable the assembly to act as a continuous structure. Typical connection methods include fasteners and/or rivets. Interior components are usually mounted to the walls at locations along the stringer assembly. This method is more efficient than monocoque cylinder component mounting at introducing local loads. The skin must be designed sufficiently stiff to enable sound mounting of exterior entities such as body mounted solar cells.

5.1.2.2 Materials

Satellite structural designs also use several different materials. Materials are chosen based on their properties, cost, and complexity. There are two typical materials used in spacecraft.

Metals

Aluminium alloys are the most widely used metallic materials in spacecraft manufacturing. The advantages include high strength to weight ratios, high ductility and ease of machining. The stiffness to weight ratio is comparable to steel; however, the strength to weight ratio is typically higher. The disadvantages include low hardness and a high coefficient of thermal expansion (CTE). The alloys are typically tempered to increase the material strengths. Two typical alloys used in manufacturing are 6061-T6 and 7075-T7. Aluminium 6061-T6 contains silicon and magnesium which strengthens the alloy during tempering. This alloy has good machinability and corrosion resistance. Aluminium 7075-T7 contains zinc and trace amounts of magnesium. The alloy exhibits higher strength than 6061-T6, but is more difficult to machine.

Beryllium is used for very high-stiffness aerospace applications. It has a specific modulus 6.2 times the specific modulus of aluminium. The material is non-isotropic due to its grain alignment and therefore exhibits low ductility and fracture toughness in its short-grain direction. It is commonly used in lightweight optics and mirrors because it performs well at cryogenic temperatures (i.e. low CTE and high thermal conductivity). However, beryllium is expensive, difficult to machine, and sparsely available in the US. Beryllium must be

machined in a controlled environment because its powder is a known carcinogen when inhaled. The parts may be safely handled once machined.

Steel is mainly used in aerospace applications where low-volume strength and stiffness are important. Steel provides high wear resistance; however it is generally difficult to machine and is not efficient for structural stability. Steels are combined with many trace elements to address a wide range of needs. Austentic stainless steel is by far the most abundant steel alloy used in spacecraft. It contains 12% chromium which results in a tough chromium-oxide coating that protects parts from corrosion. Stainless steel is non-magnetic and certain low-carbon alloys can be welded without sensitization. Stainless steels are generally used for fasteners and mechanisms whereas many heat-resistant alloys are used for heat shields, rocket nozzles, and other high-temperature applications.

Titanium and titanium alloys are used for applications requiring very high strength materials. The materials exhibit high strength to weight ratios, low coefficients of thermal expansion, and excellent corrosion resistance. However, they are difficult to machine and some alloys exhibit poor fracture toughness. Ti-6Al-4V, which contains 6% aluminium and 4% vanadium, is the most popular titanium alloy used in aerospace applications. The alloy has heritage in wings and missile bodies. Perhaps its most famous applications are the castings used to connect the external fuel tank to the Space Shuttle and its boosters.

Fiber Composite Structures

Composite structures consist of a matrix and reinforcement. The matrix (metal, epoxy) binds the reinforcing fibers (carbon, graphite) together into a continuous system. The efficiency of composite structures is due its high specific modulus and unique load path. The flexural shear loads are transferred from the matrix to axial loads on the high-strength fibers, creating a structure 3 to 5 times as stiff as aluminium at 60% of the mass. These fibers may be both discontinuous and continuous entities. Discontinuous-reinforced composites are comprised of ceramic or fiber particles that are randomly distributed throughout the matrix. Aluminium reinforced with silicon carbide particles is the most widely used discontinuous composite. The majority of continuous-fiber composites are generally called laminate composites. Laminate composites are manufactured from several layers of woven fibers called laminae. The laminae are composed of several parallel fibers arranged in sheets. The sheets themselves are anisotropic and have few structural applications. However, stacking several of the laminae

with fibers aligned at different angles, called lamina angles, creates a more stable laminate composite structure. The laminate may be customized for individual applications by varying the fiber type and the lay up. For example, some graphite/epoxy laminates are tailored to have a nearly zero CTE and others may be laid up to exhibit extraordinary specific stiffness properties. Polymer-matrix composites (PMCs) are the most widely used continuous-fiber composites used for spacecraft. The matrices consist of two polymers: thermoplastics, and thermosets. Thermoplastics may be remelted and solidified multiple times whereas thermosets are not reusable after curing. These properties enable a multitude of bonding techniques and lay up procedures, many of which are currently proprietary. The downside to fiber composite structures is the large development cost required for reliable manufacturing. The large cost is due to the sensitivity of adhesive bonding to process variables. This sensitivity makes each part a unique entity which must be tested to verify strength. NASA and other programs require extensive testing of fiber composite flight hardware to verify its structural integrity. The requirements typically create the need to fabricate a protoflight structure dedicated to qualification testing followed by acceptance testing of the flight article. This qualification procedure presently prohibits the use of fiber composite structures on small-budget programs.

5.1.3 Structural Optimization Methods

Several methods are available to optimize the structural properties of spacecraft. The optimum method may vary depending on the design task. We present three of the most widely used methods: sandwich structures, multifunctional structures, and isogrid. We examine all of the technologies and their benefits for satellite structural designs. We conclude with a description of isogrid and a literature review of past research conducted in this field.

Sandwich Structures

Sandwich structures are often used in skin-frame designs. A sandwich structure consists of two thin face sheets attached to both sides of a lightweight core. The design of sandwich structures allows the outer face sheets to carry the axial loads, bending moments, and inplane shears while the core carries the normal flexural shears. Sandwich structures are susceptible to failures due to large normal local stress concentrations because of the heterogeneous nature of the core/face sheet assembly. Component mounting must therefore use potted inserts to distribute the point loads from connections. Sandwich panel face sheets are commonly

fabricated using aluminium or graphite/epoxy composite panels. The core is typically fabricated using a honeycomb or aluminums foam construction.

Honeycomb sandwich paneling is the lightest option for compressive or bending loading specific applications. Honeycomb sandwich cores are manufactured using thin strips formed into honeycomb cells. The honeycomb geometry is non-isotropic with greater stiffness in the longitudinal direction. However, the core acts nearly isotropically for in-plane loads when assembled in a sandwich configuration. The disadvantages of using honeycomb cores are the potted inserts required for mounting and the thermal inefficiencies. These inefficiencies stem from the low thermal conductivity of the adhesive layers used in construction and make honeycomb prohibitive in optical and mirror aerospace applications.

Aluminium foam sandwich panels use a porous aluminium foam material for the core. The flexural shear stiffness dominates the overall panel stiffness for relatively small panels (i.e. less than 50 inches). Therefore, the core design is an integral part of the sandwich panel design for small spacecraft. The shear stiffness of foam core sandwich panels is generally less than that of honeycomb core sandwich panels of equal mass. However, radial ribs and shear rings may be embedded in the core to overcome the low shear stiffness. A major benefit of aluminium foam construction is an increase in thermal efficiency because the core may be brazed to aluminium face sheets rather than epoxied. Brazing provides a continuous thermal path through the material which benefits applications such as cryogenic mirrors and solar arrays.

Multifunctional Structures

Multifunctional structure (MFS) technology incorporates several functions into the primary structure of a spacecraft. The main goal of these members is to minimize parasitic mass by incorporating chassis, cables, connectors and thermal control components into the satellite primary structural walls (see Figure 5.3). The walls are typically constructed out of fiber composites or sandwich panels, and the electrical components are embedded during manufacturing. The traditional ground plane/printed circuit board design is performed by copper/polymide (CU/PI) patches, multi-chip modules (MCMs), and the current cabling functions are performed using CU/PI flexible jumpers. The design allows for an easily accessible, removable, and modular electrical system [13]. The benefits of this technology include a 70% reduction in electronic

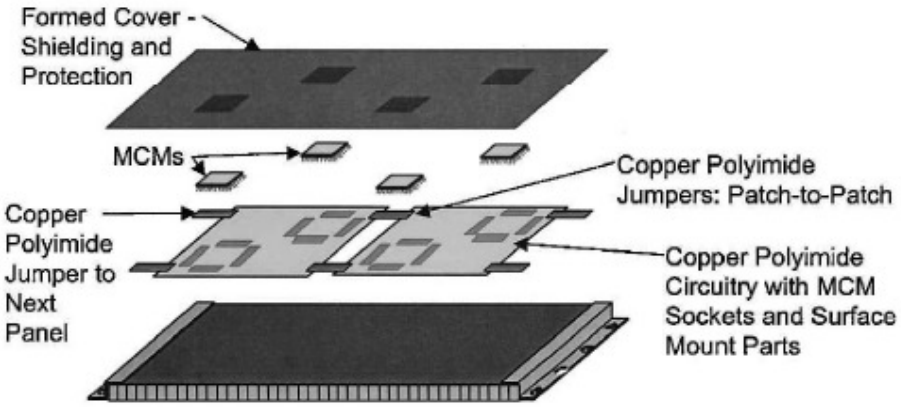

Figure 5-3 Schematic of MFS Configuration

enclosures and harnesses, a 50% reduction in space craft volume required for these conventional components, a reduction in labour required for spacecraft assembly, and an extremely robust system with wide applicability to several missions. Lockheed Martin has recently proven the technology as an experiment aboard the Deep Space 1 mission.

5.1.3.1 Isogrid Structures

Isogrid uses an array of equilateral triangle cut outs to increase the stiffness per weight of a structure. The pattern may be manufactured by machining a metallic panel, or it may be constructed using fiber composite materials. The concept began in the early 1960s using metal structures and development continues today with research focusing primarily on composite applications.

5.2 FE Model Generation of the Satellite

To reach the stated objective of this practical phase of the project, design criteria for the satellite structure was defined. These criteria included

- Significant over testing must be present,
- The natural frequencies should be in the 2-60 Hz frequency range,
- The test structures should be easy to analyze,
- The acceleration environments should be within the acceptable specification of the test shaker.

Structural Configuration

The Satellite structural configuration is designed to accommodate all of the mission components or payloads (Figure 5.4). The structural assembly consists of ten plates. The two end panels are hexagonal plates measuring 50 mm in major diameter and 4 mm in thickness. The two payload panels are hexagonal honeycomb plates measuring 6 mm in thickness. The side panels are formed using 2.5 mm thick plates. The frames reinforce the side panels and solar panels which measure 1500X500X4 mm and provide a stiff, stable surface to affix solar cell arrays.

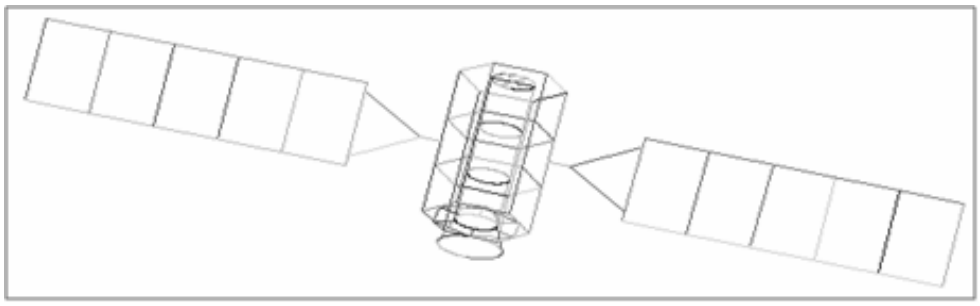

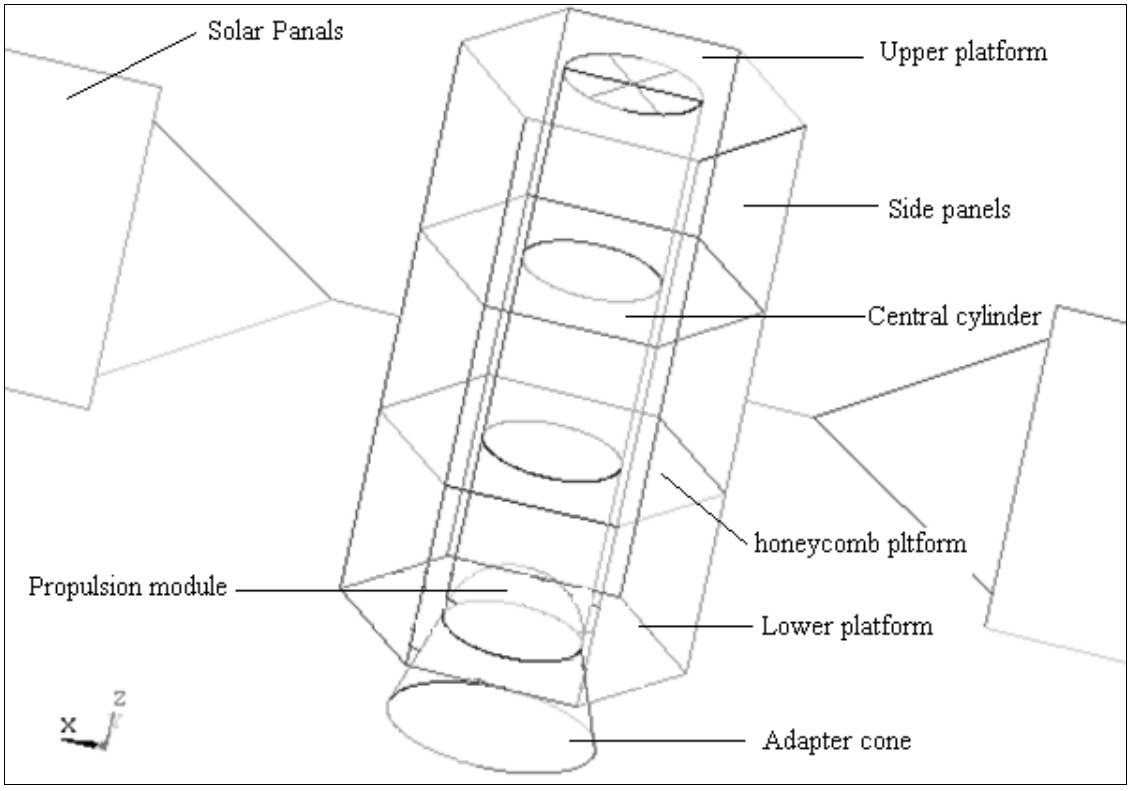

Figure 5-4 Geometry model of the satellite model

5.2.1 Geometry Modeling

Figure 5.4 is a drawing of the Satellite that was built. The geometry for a Satellite was created on ANSYS by defining key points, lines, areas, volume.

The Satellite is made of many thin structures, which is defined as area in the model and frame structure, which is defined as line. Some of the secondary structures, such as the propulsion module is defined as a sphere volume attached with a ring to the lower platform and scientific payloads are defined as a key point attached with the supporting beam structure on the honeycomb platform. The model will be initially broken up into seven groups, each representing a separate piece of the structure. These groups include: lower platform, upper platform, honeycomb platform, solar panels, adapter cone, side panels, central cylinder, and frame geometry.

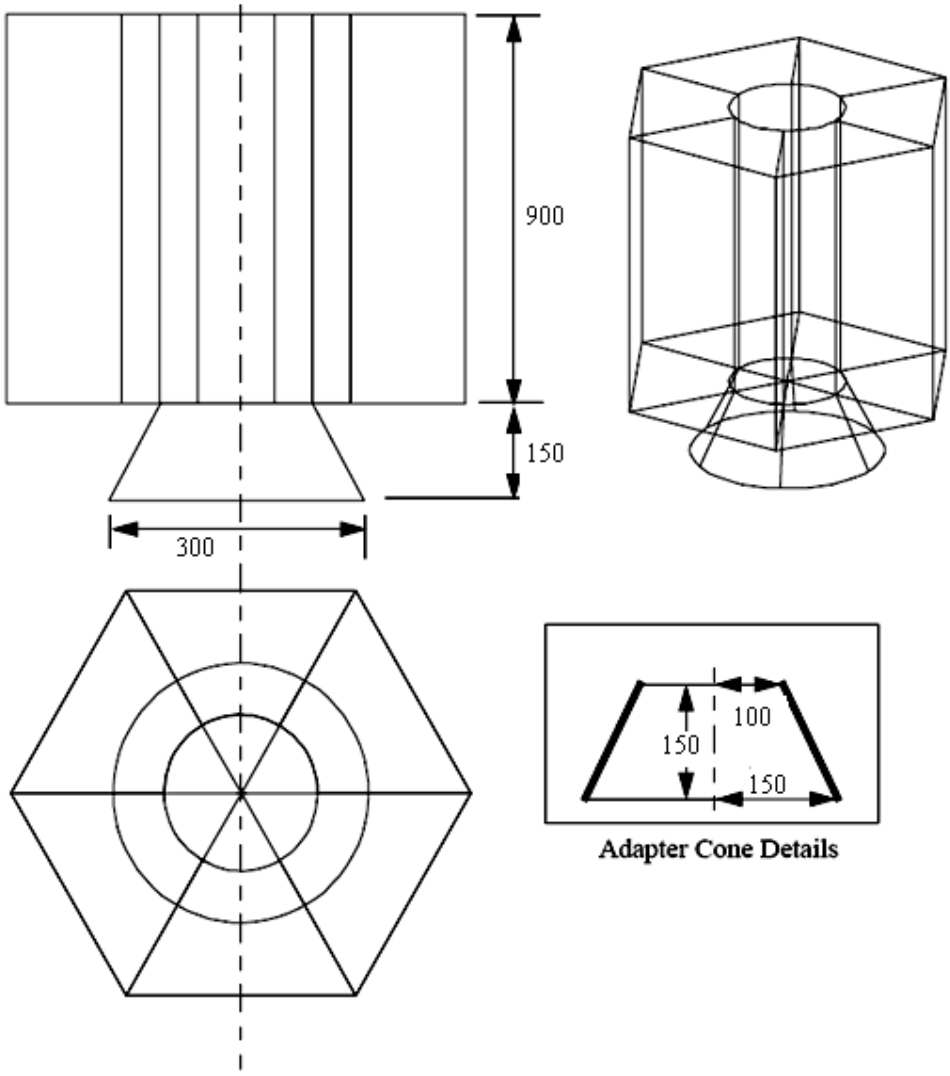

Figure 5-5 Geometry specifications for the Satellite (dimensions are in mm).

5.2.2 Finite Element Model

In this section, it is defined a finite element mesh for the Satellite model that was developed earlier.

First material property is defined by creating Isotropic materials, named titanium and aluminium, which uses a Linear Elastic Constitutive Model. The material's Elastic Modulus, Poisson's Ratio and Density are 110.4 GPa, 0.16, 7474 Kg/m^3, and 72.45 GPa, 0.33, 2796 Kg/m^3, respectively.

Then the element type and real constants are defined for idealizing the different components of the satellite. Therefore for the thin structures such that the lower and upper platforms are idealized as a plate element. The scientific platform is a honeycomb structure which is idealized as a plate element by calculating the equivalent thickness of the plate given by eqn. (5.1)

$$t_{eq.}{}^{3} = 12(1 - \nu^{2})I \tag{5.1}$$

where $t_{eq.}$ is the equivalent thickness of the plate

ν is the Poisson's Ratio of the honeycomb

I is the moment of inertia of the honeycomb

The scientific payloads of the satellite model are idealized as concentrated masses. The concentrated masses will be modeled with Point Elements. It is also applied a rigid element to model propulsion module.

The real constants will include properties for 2-D shell elements, 1-D frames, 3-D solid, and 0-D concentrate masses and the assignemet of the material properties for the components is shown in table 5.1.

Additionally, it is created a field to define a thickness variation in the Adapter cone. The thickness of the cone will be 5 mm at its base and will vary linearly to a thickness of 10 mm at its top dimension as shown in fig. 5.6.

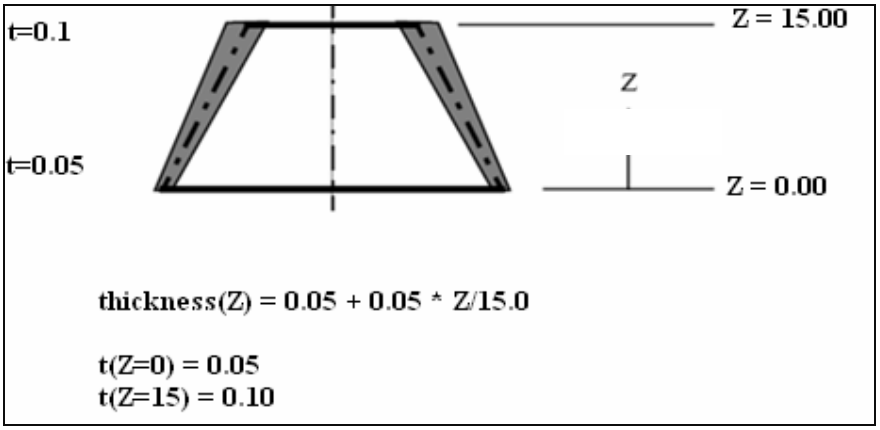

Figure 5-6 Adapter Cone's specifications - 2D slice (dimensions are in cm)

Component	Material type	Real constant	Material
Central cylinder	Shell 63	T = 4 mm	Aluminium alloy
Adapter	Shell 63	T = 5-10 mm	Titanium alloy
Upper platform	Shell 63	T = 2.5 mm	Aluminium alloy
Lower platform	Shell 63	T = 4 mm	Aluminium alloy
Honeycomb platform	Shell 63	T = 6 mm	Aluminium alloy
Side panels	Shell 63	T = 2.5 mm	Aluminium alloy
Solar panels	Shell 63	T = 4 mm	Aluminium alloy
Propulsion block	Solid 164	m = 360 Kg	Aluminium alloy
Payloads	Mass 21	m = 640 Kg	Aluminium alloy
Payloads supporting beam	Beam 4	Hollow box 50X50X2.5 mm	Aluminium alloy
Main structure frame	Beam 4	Angle iron 50X50X2.5 mm	Aluminium alloy
Solar panel frame	Beam 4	Angle iron 40X40X2.5 mm	Aluminium alloy

Table 5.1 The Element Property assignments

Finally the model is meshed: first by attributing element types, real constants and material properties to the geometric model; then by setting mesh size control and generating the mesh.

Note that to attain connectivity between the nodes of different elements it has been made all the elements to have the same Degree Of Freedom (DOF) and each node to overlap.

5.3 Defining Boundary Condition

It is assigned Boundary conditions to the model and set up two boundary conditions; launch and test attachment for the loading conditions of dynamic analysis and Static analysis respectively.

A simply supported displacement constraint, named Launch constraint (used for static analysis), for all vertices on the outside edges of the Upper and Lower Platforms (i.e., ball joint) is created. The displacement is fixed in translation and free in rotation. Test constraint (used for dynamic analysis) is made by a fixed support displacement constraint by setting zero in translation and rotation for all vertices on the outside edges of only the lower platforms.

Finally, it is defined two Load Cases for this model. One Load Case contains only the Launch constraints and is use for static analysis. Another Load Case contains the Test constraints meant for the dynamic analysis.

5.4 Static and Spectral Analysis of the Satellite

5.4.1 Static Analysis

Static analysis is done for an inertial loading created due to the launch accelerations. It is defined a loading, of 14g load in the Z direction. It should be noted, the gravity constant for this problem is 1 g = 9.81 and the inertial loading is applied to the entire model.

5.4.2 Spectral Analysis

Spectral analysis is done for a test condition of swept test where the excitation is in the form of a sinusoidal except that the frequency and magnitude are varied slowly. The frequency is swept slowly from a low frequency 2 Hz to an upper frequency limit, between 4 and 40Hz and in the downward direction up to 60 Hz. Constant peak accelerations between 1g to 14g is applied as shown in figure (5.7) below. To apply these dynamic loads spectral analysis is done.

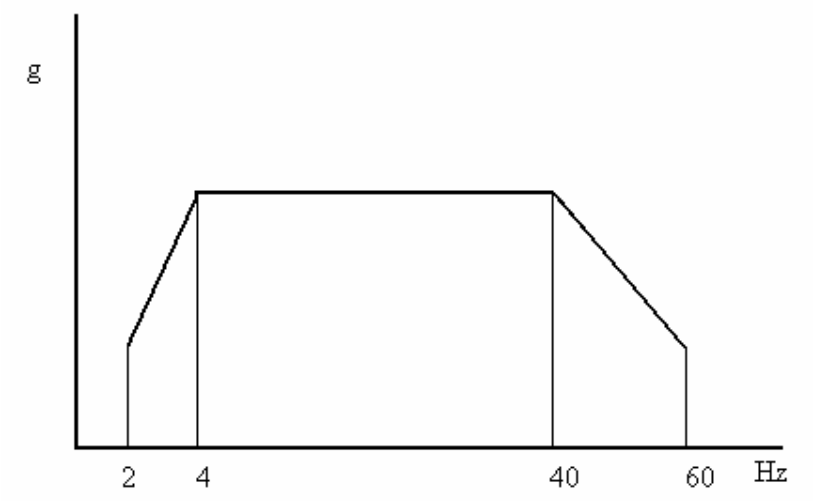

Figure 5-7 Curve Showing the Input versus Forcing Frequency

A single-point response spectrum (SPRS) analysis is used because, we specify one response spectrum curve (or a family of curves) at a set of points in the model, such as at all supports, as shown in Figure (5.8).

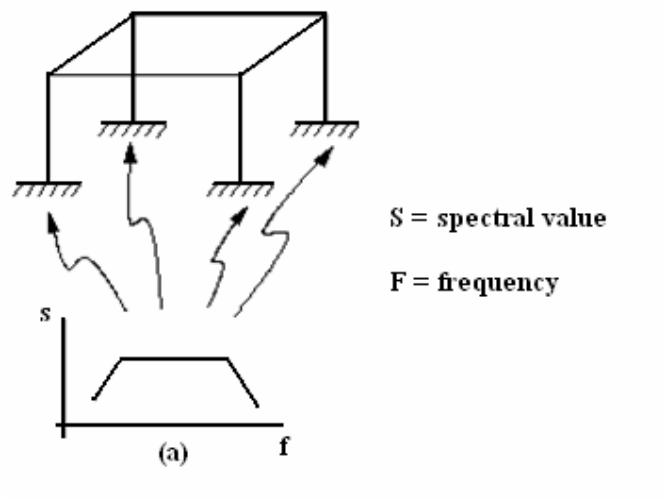

Figure 5-8 Single-Point Response Spectra

The procedure for a single-point response spectrum analysis after building the model consists of five main steps:

1. Obtain the modal solution.
2. Obtain the spectrum solution.
3. Expand the modes.

4. Combine the modes.
5. Review the results.

Obtain the Modal Solution

To determine natural frequencies normal mode analysis is done. The standard Block Lanczos algorithm available in ANSYS is used, which extracts the required eigenvalues of a matrix. The number of modes extracted should be enough to characterize the structure's response in the frequency range of interest.

Obtain the Spectrum Solution

ANSYS offers the Single-point Response Spectrum (SPRS) for a spectrum analysis. Not all modal analysis options and not all eigenvalue extraction techniques work with all spectrum analysis options.

Enough modes to cover the frequency range spanned by the spectrum and to characterize the structure's response were chosen. The accuracy of the solution depends on the number of modes used: the larger the number, the higher the accuracy

Spectrum type is acceleration and the Excitation Direction is in the Z coordinate. Spectral-Value-Versus-Frequency Curve of figure 5.6 is applied.

The output from the solution includes the participation factor table. The participation factor table, which is part of the printed output, lists the participation factors, mode coefficients (based on lowest damping ratio), and the mass distribution for each mode. To obtain the maximum response of each mode (modal response), multiply the mode shape by the mode coefficient. We can do this by retrieving the mode coefficient with the GET command and using it as a scale factor in the SET command.

Expand the Modes

Then mode expansion as a separate solution pass after performing the spectrum solution was performed. It is used to selectively expand (write mode shape to the result file) significant modes. Only expanded modes are used for the mode combination operation in the subsequent mode combination pass.

It expands only those modes whose significance level exceeds the *SIGNIF* threshold. The significance level of a mode is defined as the mode coefficient of the mode, divided by the maximum mode coefficient of all modes. Any mode whose significance level is less than *SIGNIF* is considered insignificant and is not expanded. The higher the *SIGNIF* threshold, the fewer the number of modes expanded. Therefore a *SIGNIF* 0.001 is taken for this problem.

Combine the Modes

ANSYS offers five different mode combination methods for the single-point response spectrum analysis. But Square Root of Sum of Squares (SRSS) is used. These combine the maximum modal responses by using the specified mode combination method to calculate the overall response of the structure.

Review the Results

Results from a single-point response spectrum analysis are written to the mode combination file. These commands calculate the overall response of the structure by combining the maximum modal responses in some fashion (specified by one of the mode combination methods).

The next chapter describes a detailed result of the static and dynamic analysis of the case study for a specific satellite, an analytical method of the notch predictions are conducted followed by the result of the ANSYS.

Chapter Six: Results of Static and Dynamic Analysis

This chapter contains plots of the stress contours obtained in the static and dynamic test finite element analysis. Both the shell stresses and beam stresses are plotted. The results shown are the Von-Mises stresses and the total displacements calculated in the analysis. Keep in mind that the unit of all the ANSYS results now on wards are in SI units.

The mesh shown below is the frame of a satellite modeled as beam and plate elements, specifically consisting of 7140 elements and 6009 nodal points. The structure optimum weight has been calculated equal to 1031 kg.

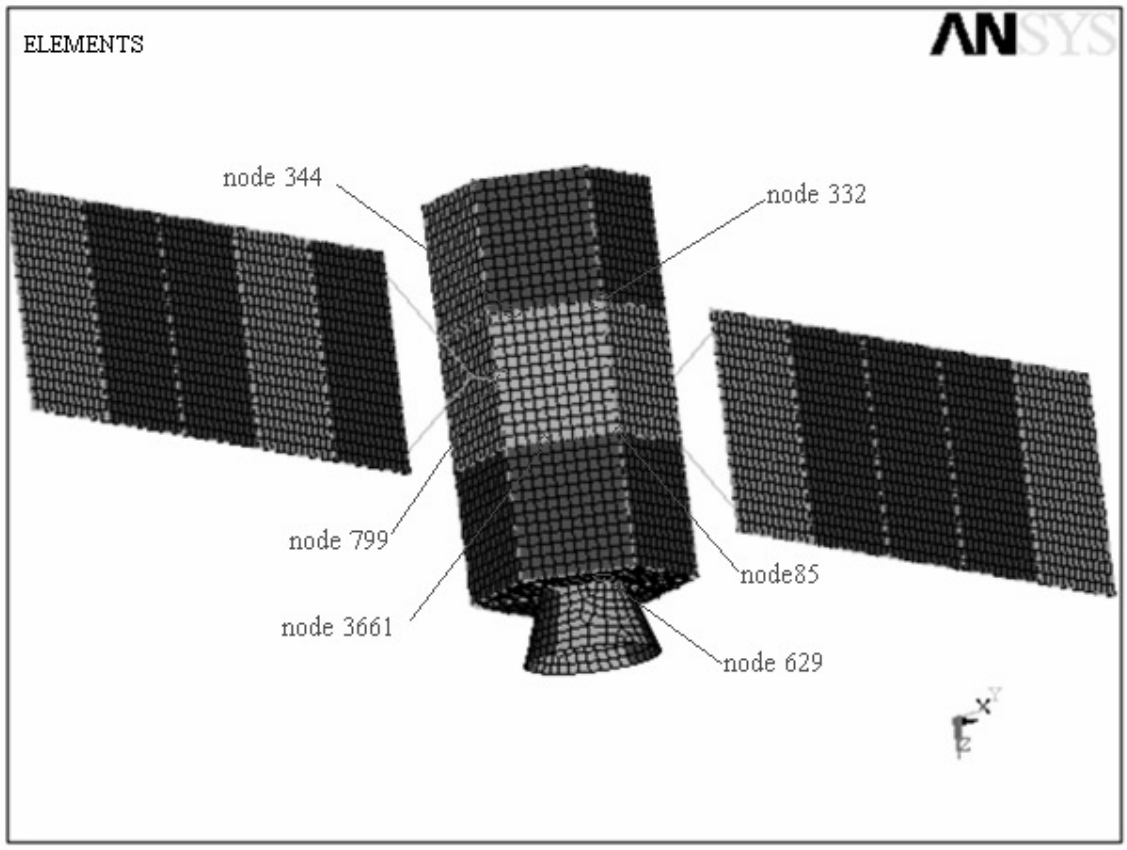

Figure 6-1 FE Model of the Satellite

6.1 Static Analysis

In the static analysis, 14g inertia load has been applied on the satellite model in the axial direction, and the end corners of the upper and bottom platform have used as fixed points only for translation for boundary condition of launcher attachment. After several runs, the optimum value for the discussed geometric parameters has been finalized with a safety factor

equal 4 for the maximum von-mises stress of 54.7 MPa and yield strength of the material is 200 MPa. Therefore the structure is found safe where the margin of safety for satellite structure is 1.05. The highest stress value is observed in the side panels where the connections of the solar panels' frames are made (fig.6.2).

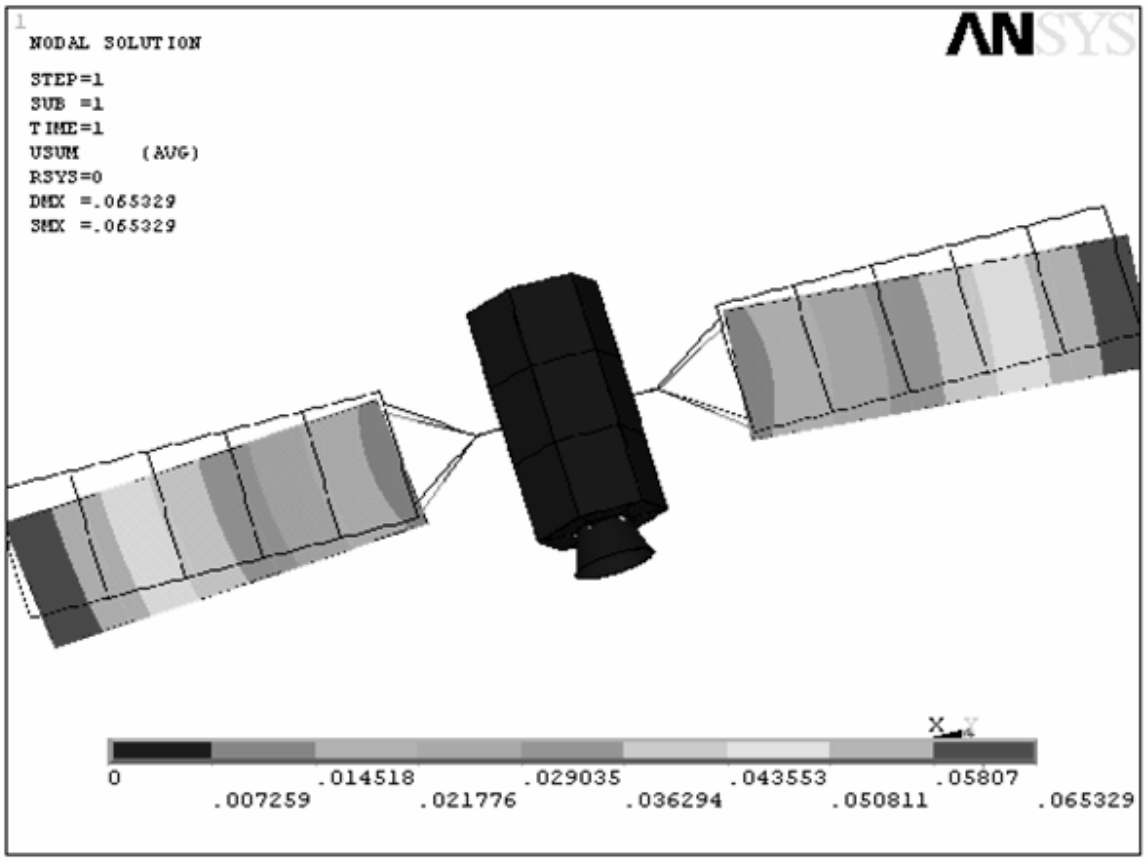

Figure 6-2 Total Displacement Stress in the Space Satellite

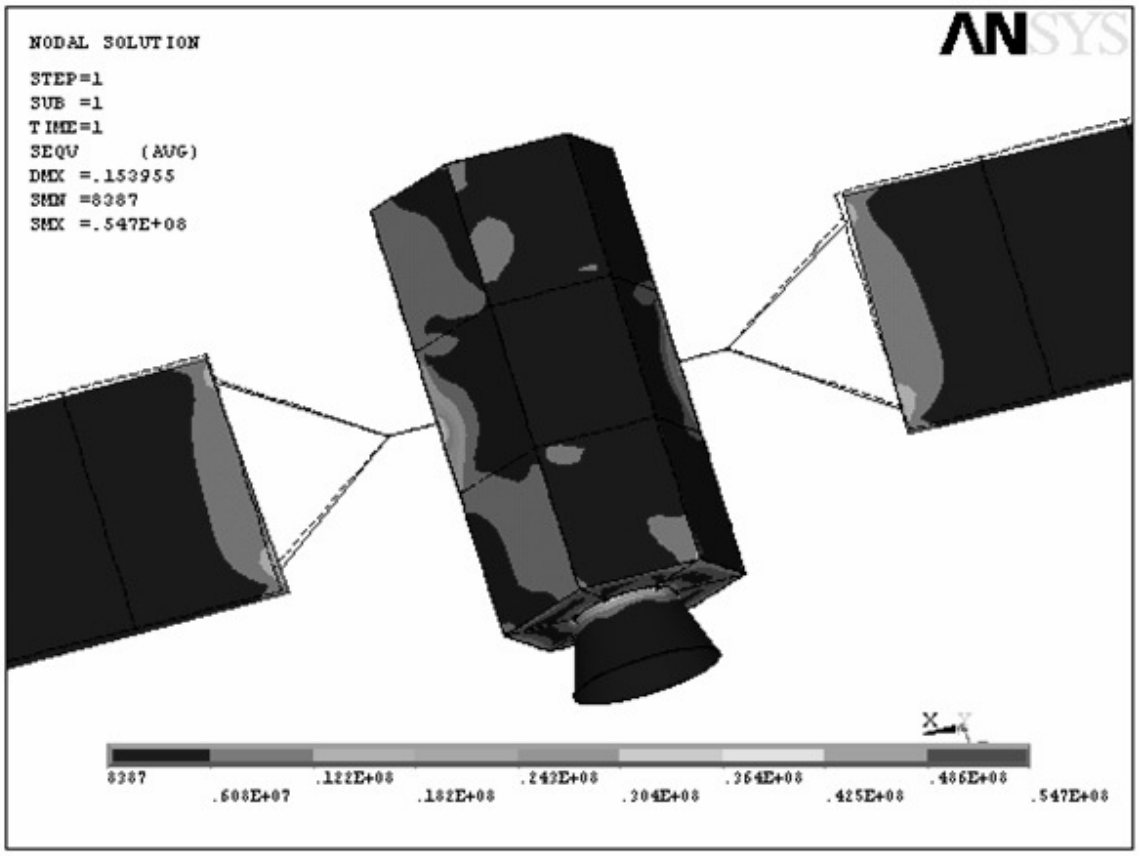

Figure 6-3 Von-Mises Stress in the Space Satellite

6.2 Modal Solution of Vibration Test

The goal of modal analysis is to determine the natural shapes and frequencies of the structure during free vibration and to determine the response of a structure due to dynamic loads. This modal approach is popular due to its efficiency and can approximate the response using only a small number of modes. When dealing with small models all the modes in the frequency range of interest are included for the response solution. But for larger structures, including all the modes in the frequency range can be computationally expensive. Therefore it is important to understand the modes with large contributions to the overall response of the structure.

The first step in calculating the modal frequency response is to compute the normal modes of the structure. The results from the normal modes analysis are the mode shapes and natural frequencies. Observing the mode shapes reveals how the structure will deform at natural frequencies. However, the modal displacements / deformation information does not provide a

good insight to the response since the Eigenvectors are arbitrarily scaled and the displacements seen in the postprocessor can be deceiving.

The next images are that of the 4 modes of this satellite during free vibration. This problem can be seen as a depiction of the likeliest deflections a satellite would take during a base excitation; since in most satellite the first four modes preferably used. As expected, the first mode is a swaying of the satellite panels from up to down. The second, mode is swaying of the honeycomb platform. The third mode is the swaying mode of the adapter cone. The fourth mode is a stretching and compression mode in the vertical z direction.

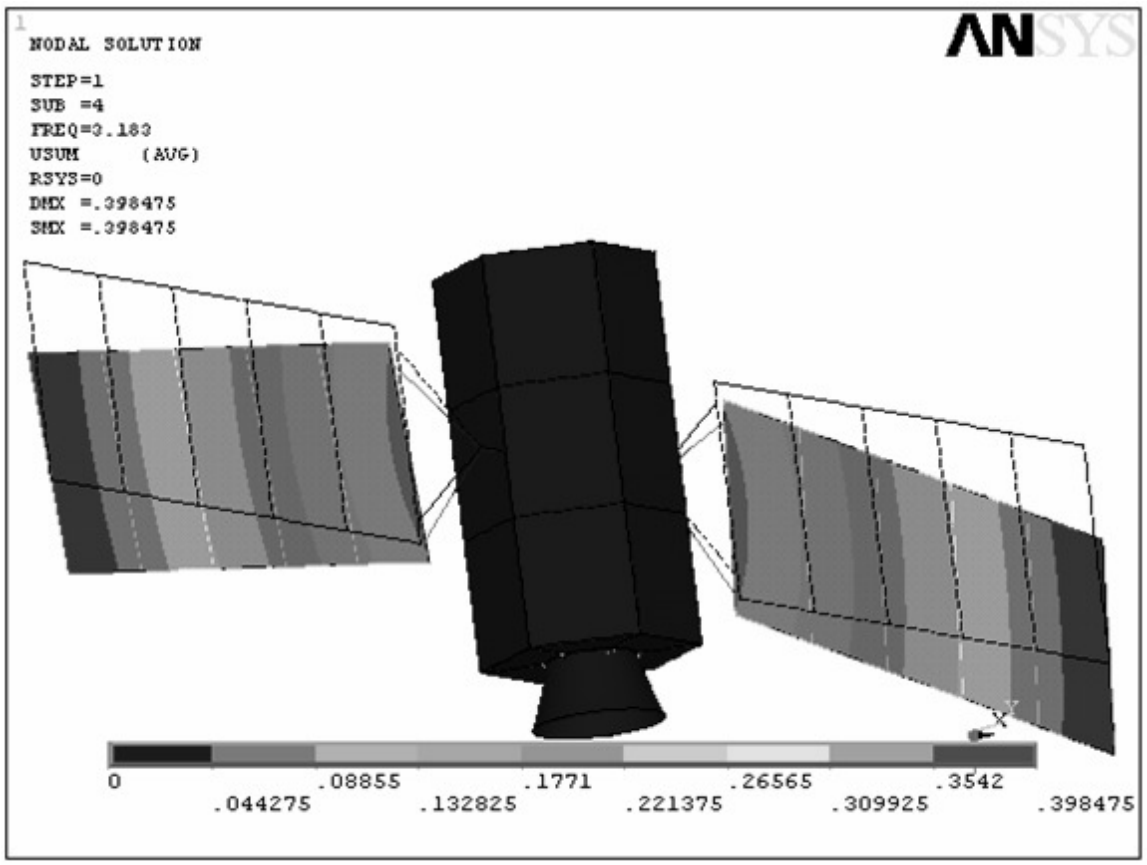

Figure 6-4 Swaying Front to Back of the Solar Panels

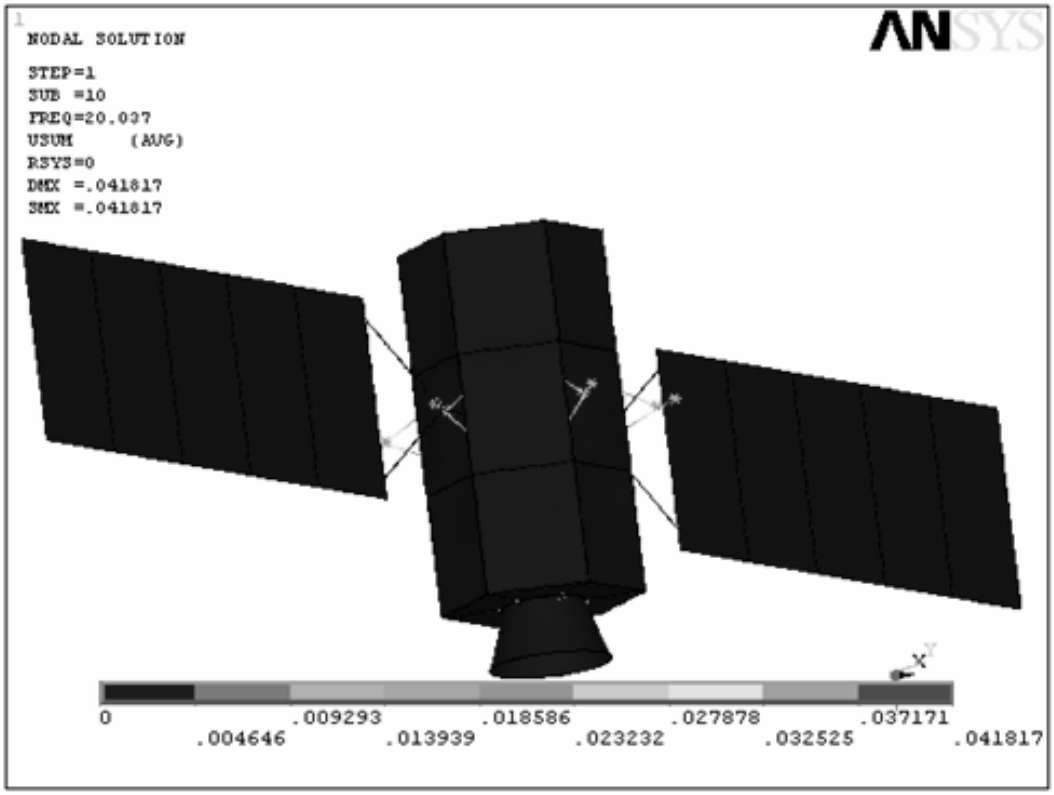

Figure 6-5 Swaying of the Honeycomb Platforms

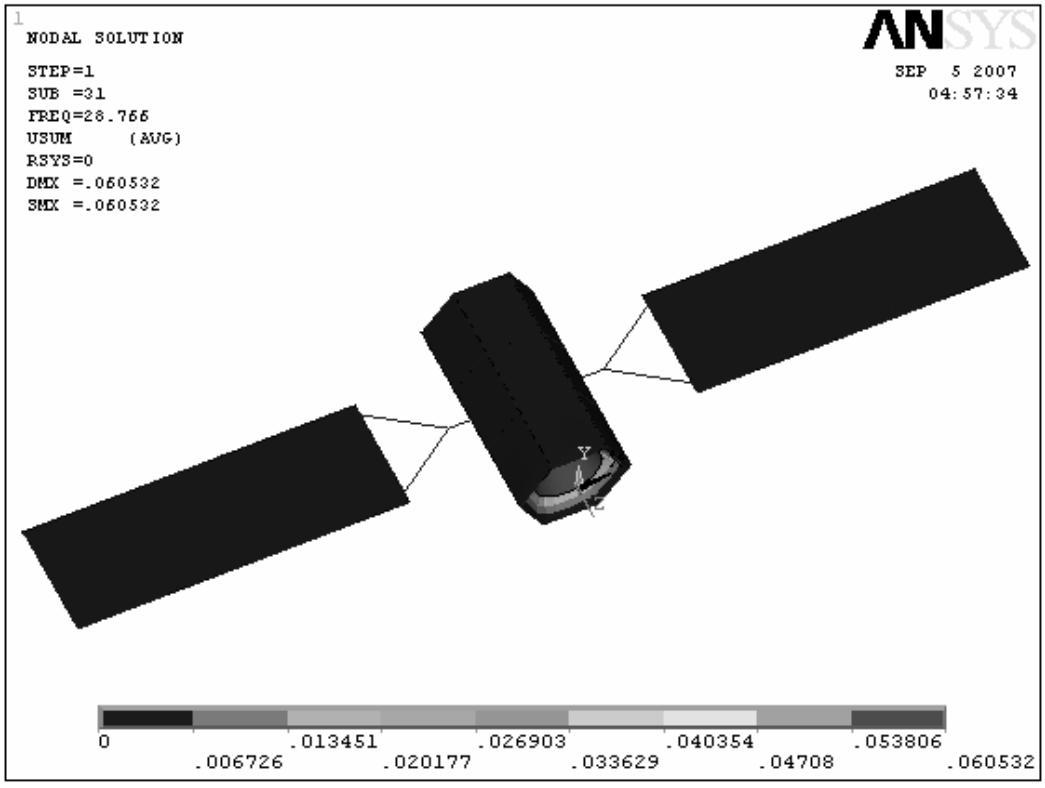

Figure 6-6 Swaying of the Adapter Cone

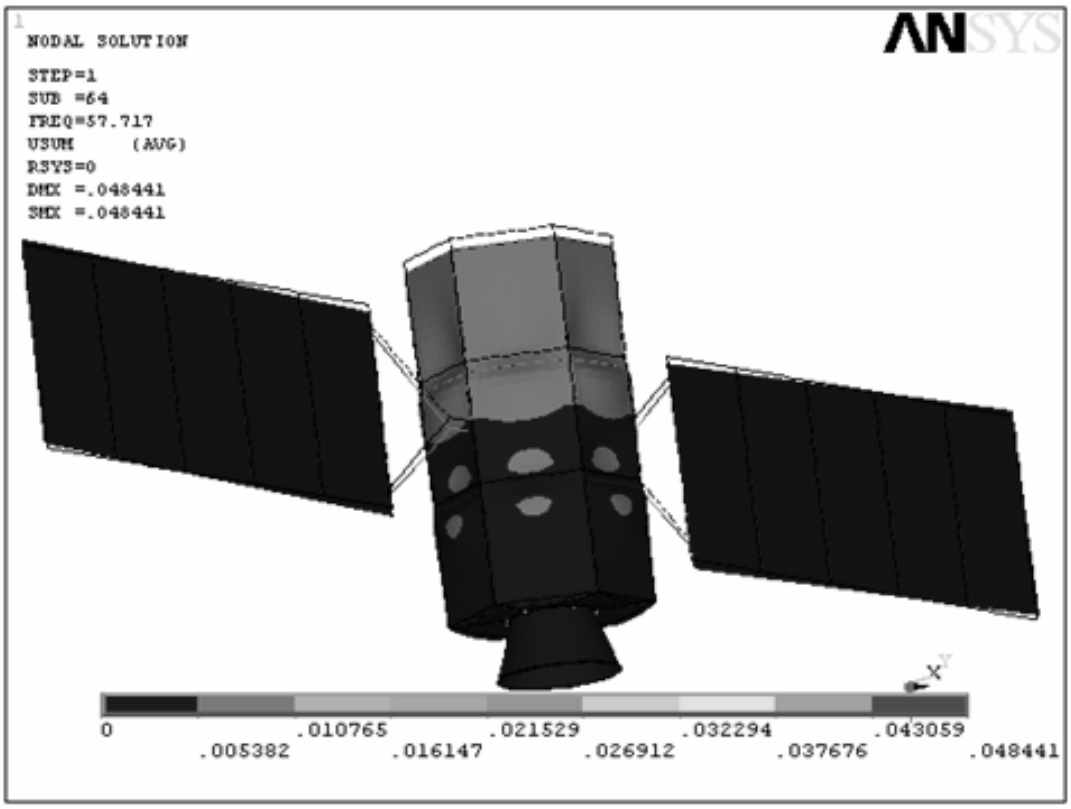

Figure 6-7 Drum Type Mode

The modal effective mass associated with each deformation mode represents the amount of system mass participating in that mode. Therefore, a mode with a large effective mass is usually a significant contributor to the system's response. These criteria are in other words used to find the important system modes. A typical requirement for the selection of target modes is that modes with a translational effective mass equal to or greater than 2 percent of the total mass are target modes.

The normal modes analysis is performed for a frequency range of 2 Hz to 60 Hz. The modal effective mass can be printed out during the normal modes solution. A trial run is conducted to determine the number of modes needed to represent the response of the entire structure. One way to determine this is to calculate the cumulative modal effective mass. If the cumulative sum of modal effective mass is more than 80%, then the modes are sufficient to represent 80% of the response of the structure. In some applications, the requirement is to use 95%. The modal effective mass table is printed out along the direction of the excitation as shown in table 1. The sum along the direction should be compared with the total mass of 1030 Kg.

The results of the analysis are shown in table 1 and figure 1. It can be seen that modes 4, 9,10,12,31 and 64 represents 97 % of the response in Z direction. A quick review of the table reveals that, for most applications it is just sufficient to consider the first 64 modes of the structure to simulate the frequency response of the entire structure.

mode	frequency	participation Factor	Modal effective mass	mode coefficient	percentage contribution
4	3.183	3.615	13.06823	5.302	1.2675291
9	20.03	-8.177	66.86333	-7.23E-03	6.4852889
10	20.04	-1.017	1.034289	-8.98E-04	0.100319
12	20.73	-0.09637	0.009287	-7.95E-05	0.0009008
31	28.77	-16.7	278.89	-7.16E-03	27.050436
64	57.72	25.3	640.09	6.69E-04	62.084384

Table 6.1 Modal Effective Mass

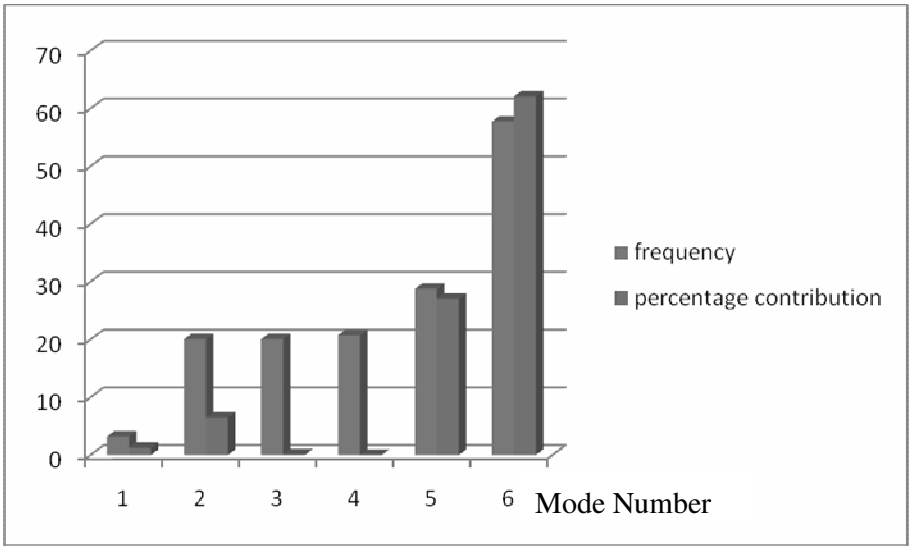

Figure 6-8 Modal Contributions in the Z Translation (for the chosen input load)

6.3 Dynamic Analysis

This section presents the dynamic response produced by the test item during the test configuration. It is important to note that this configuration is completely used to study the phenomena of the response of the satellite by producing the boundary condition of rigid shaker table's fixture and predict the critical places and notch value using energy limiting method.

A complete dynamic structural analysis of the test structure was performed. The analysis started with a modal analysis where natural frequencies, the effective masses were computed for the satellite structure as stated in the above section. Then the analysis continued with the base-driven sinusoidal vibration analysis of the test system. This analysis is a representation of the real-life condition of test. It yields the von-mises stress of the satellite, which corresponds to the test condition of the satellite.

6.3.1 Critical Location Prediction

One or more critical Locations on the satellite for vibration testing are predicted from the response of von-mises on the nodes with a maximum stress for a specific frequency. It is quite clear that those fundamental (resonance) frequencies are with a peak stress value than other frequencies. Therefore for each fundamental natural frequency the node with the most pike von-mises stress value is taken as critical location and seen for the spectral response.

For the satellite, the dynamic base excitation that is shown in chapter 5 is utilized. The material being alloy-aluminium, we can use the "Von-mises theory of failure". So the stresses are obtained as the von-mises stresses.

Fig. 6.9 shows von-mises stress variation for nodes taken as critical location and lists the nodes with their numbers consistently to ANSYS results to locate the locations on the satellite model. Each location represents the node with maximum von-misses stress for the fundamental resonance frequencies which have higher participation as stated in above section such that 3.18, 20.03, 20.04, 20.73, 28.766 and 57.72 Hz and the respective nodes are 799, 344, 85, 3611, 629, 332 and their relative location on the model is shown on fig. 6.1. It can be seen from the relative comparison of curves of the graphs that, the stresses are maximum for node 3611 which is located at the lower honeycomb panel. For this node the peak stress within 60 Hz is 1790 MPa at resonance frequency of 20.73 Hz while the stresses induced at all elements are found absolute peak. The 4^{th} node thus is the most critical point out of the six nodes.

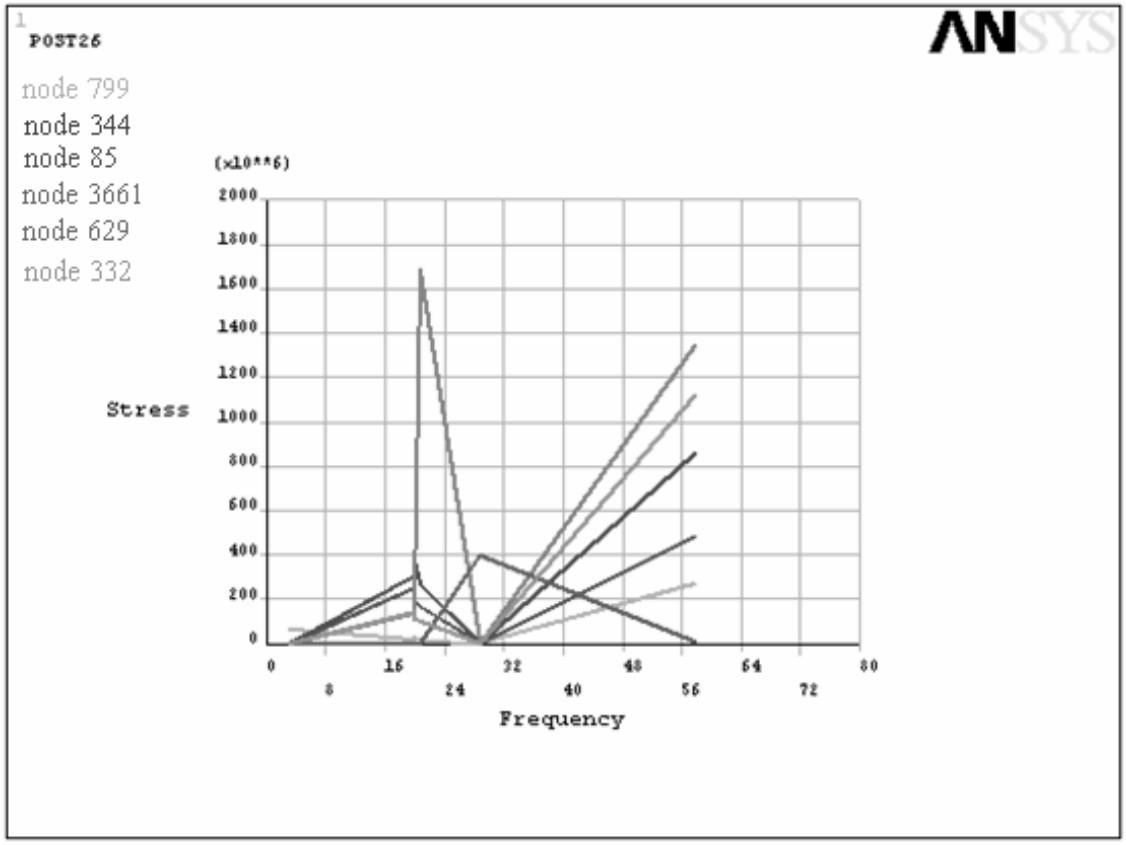

Figure 6-9 Maximum Stresses Induced for Node no. 799, 344, 85, 3661, 629 and 332

6.3.2 Notch Value Prediction Using Energy Method

For this satellite structure, only the notching of the critical elements, where the critical nodes are founded, is of interest, since these elements by far are the dominant one to predict the notch value. Also the strain energy value of the von-mises stress is a prime important parameter since it is related to the total amount of energy transmitted to the test item during the vibration test.

The strain energy at the critical element during test was determined from the von-mises stresses with the following assumption: when an element is subjected to a resultant stress due to some load the element is strained and the work done by the external applied load must be stored up in the element in the form of strain energy. The strain energy U will be given on a differential volume dv by:

$$U = \frac{1}{2}\sigma_v \varepsilon dV \tag{6.1}$$

Where σ_v is the von-mises stress and

ε is the strain.

If the element has constant cross sectional thickness t and volume v, then

$$dV = t\, dA$$

and we have the relation $$\varepsilon = \frac{\sigma_v}{E} \tag{6.2}$$

and substituting Eqns. (6.2) into eqn. (6.1) yields

$$U = \frac{t}{2E}\int_{y_{min}}^{y_{max}}\int_{x_{min}}^{x_{max}} {\sigma_v}^2\, dA \tag{6.3}$$

While the element shape is assumed as a rectangle as shown below.

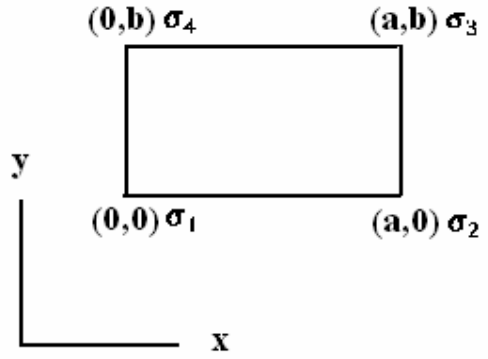

Figure 6-10 Rectangular Element

The von-mises stress can be assumed to have a form of polynomial function of x and y variables over the element like

$$\sigma_v(x, y) = a_0 + a_1 x + a_2 y + a_3 xy \tag{6.4}$$

after solving it will be

$$\sigma_v(x,y) = \sigma_{v1} + \frac{(\sigma_{v2} - \sigma_{v1})}{a}x + \frac{(\sigma_{v4} - \sigma_{v1})}{b}y + \frac{(\sigma_{v1} - \sigma_{v2} + \sigma_{v3} - \sigma_{v4})}{ab}xy \qquad (6.5)$$

This equation will be inserted into eqn. (6.3) to estimate the strain energy applied to the element and solving the double integral. Note that the detail derivation of all the equations in this section is shown in Appendix A.

Finally, energy specifications can be defined. The specification for energy is determined by substituting the stresses with the yield stress of the material to eqn. (6.3). Therefore the notching values for the elements of critical locations are shown in the table 6.2.

Elements of critical locations	Applied strain energy to the element (J)	Specific strain energy of the element (J)	Scale of notching
1st	2.225	0.216	10
2nd	3.105	0.216	14.4
3rd	3.105	0.216	14.4
4th	14.99	0.518	30
5th	17.21	1.38	12.5
6th	19.23	1.38	14

Table 6.2 Predicted Notching Value for the Critical Elements

Note that the detailed calculations of notch value of each critical element are shown in Appendix B.

Therefore we can conclude from the result that with energy limiting, the energy value of the von-misses stresses of the critical section of elements are reduced by a scale of up to 30 with a maximum of notching at a resonance of 20.733 Hz. The analysis showed that the energy specifications will significantly reduce the over testing according to the result accomplished.

The result of the von-mises stress from a single-point response spectrum analysis is shown in figure 6.10 and the peak stress is 537 Mpa and it is found at the most critical location of the 4th element. The plot is called a response spectrum of the stress which is simply a plot of the peak or steady-state response.

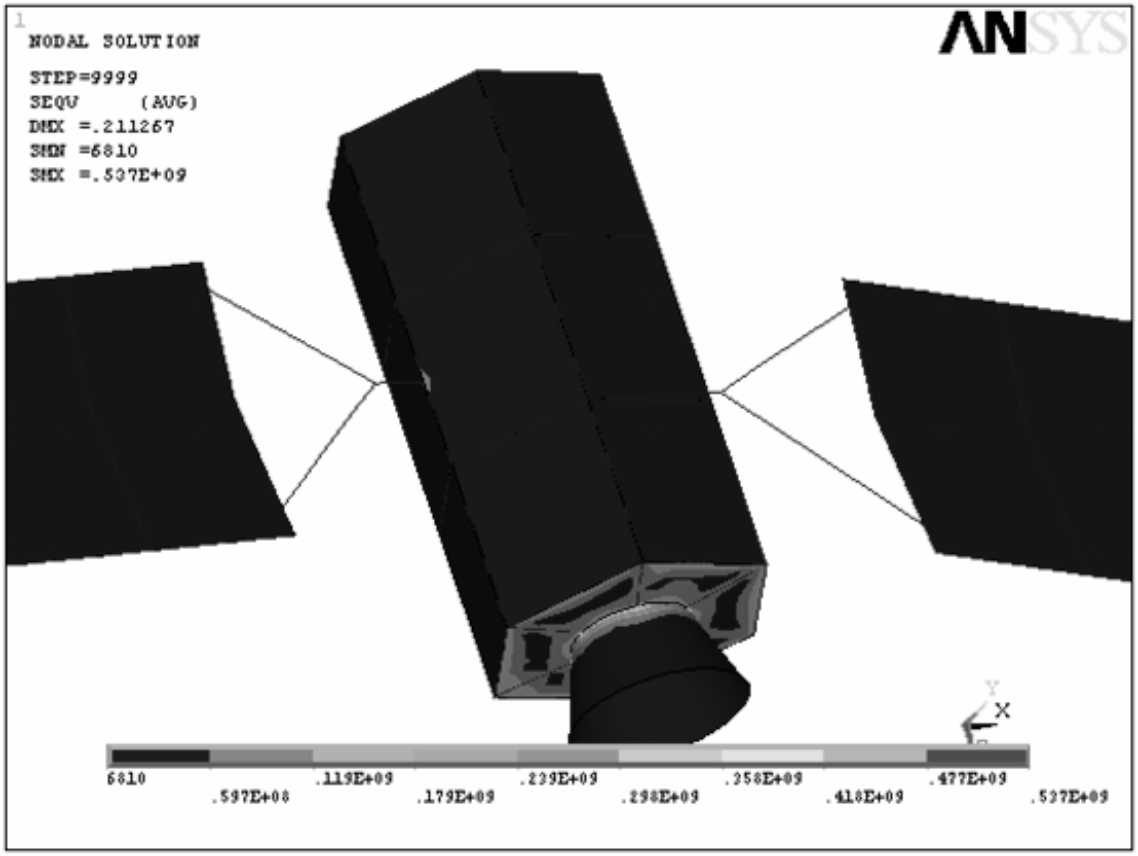

Figure 6-11 The Overall Von-Mises Stress Contour Plot for the Spectral Analysis

6.4 Verification of the Method

In this section it is considered the simple vibratory system of launch configuration of Figure 6.12, which consists of two oscillators connected in series. The main oscillator is vibrated through motion of its rigid base; the secondary oscillator is excited because of its attachment to the main one. To use terminology consistent with literatures, for example, Scharton [41], the main oscillator is referred to as the source and the secondary oscillator is the load.

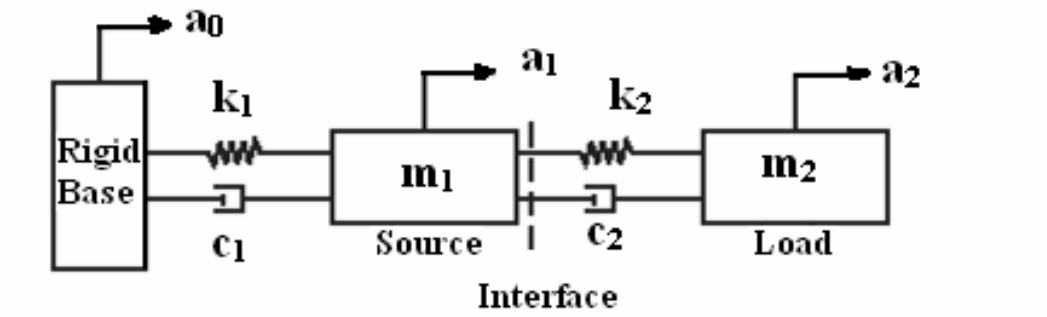

Figure 6-12 Source and Load Oscillator in Launch Configuration.

The verification of the energy limiting method when compared with the force limiting method is studied by assuming that the oscillatory system of Figure 6.12 represents a vibration mode of a flight-mounting structure (source) coupled with a vibration mode of the test article (load). For this project the mounting structure is a launch vehicle and the test article is the satellite.

As a numerical example, assume that the mass m2 is twice m1, the damping coefficient C of both oscillator is 30 N Sec/m (i.e., damping ratio of 2.5%), and the spring constant K of both oscillator is 36E6 N/m. For the launch configuration the same procedure of ANSYS is followed except that the masses are idealized as a point by an element type of MASS21 and the spring-damper is idealized as a line by using an element type of COMBIN14.

The amplitude of the coupled system interface acceleration is shown in Figure 6.13. One may observe the two peak accelerations at the system resonance frequencies located at 18 and 48 Hz. The notch in the interface acceleration at the resonance frequency of 48 Hz is clearly visible

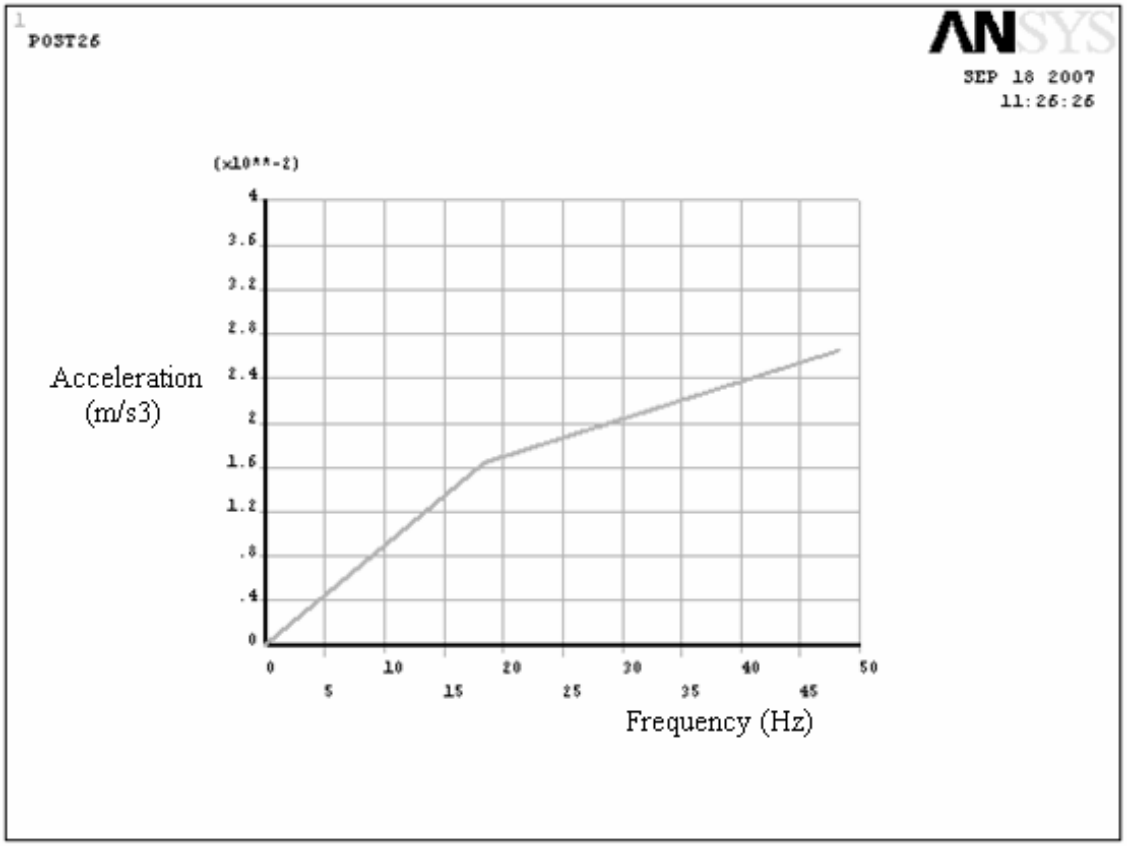

Figure 6-13 Coupled System Interface Acceleration and Test Specification.

The interface force in a coupled system (or flight configuration) is obtained by an analysis as shown in Figure 6.14. This curve also peaks at the two resonance frequencies of the coupled system, with a maximum value of 1500 KN occurring at 48 Hz.

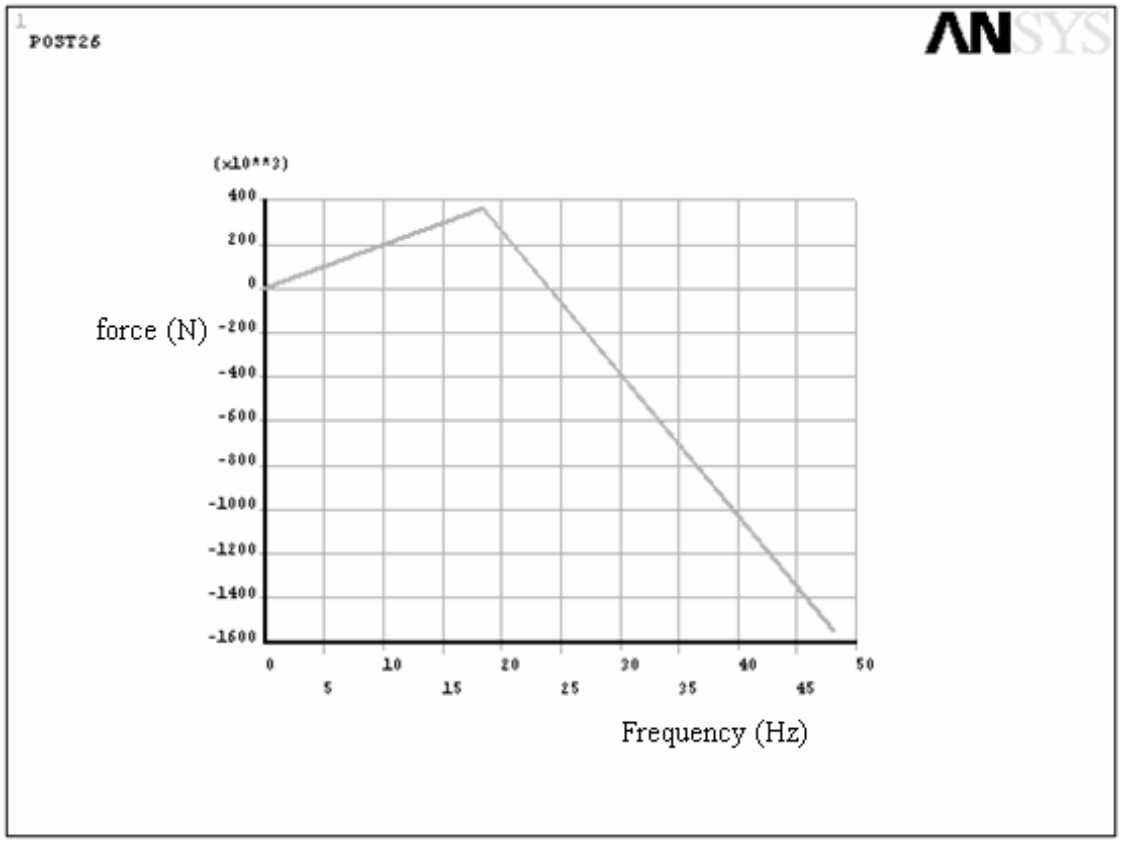

Figure 6-14 Coupled System Interface Force.

Figure 6.15 presents the reaction force produced by the test article during the test. The reaction force peaks at 57.3 Hz, with a value of 3400 KN.

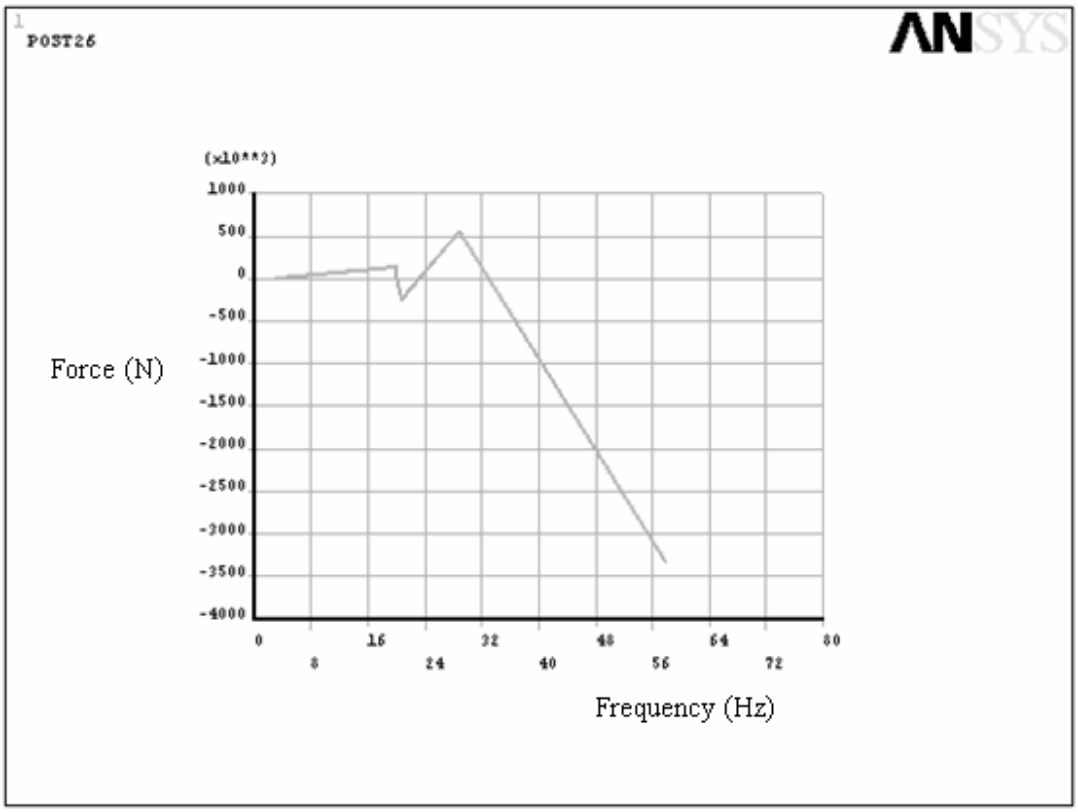

Figure 6-15 Reaction Force during Vibration Test.

A comparison of the above peak forces at the coupled system and test configurations shows that vibration testing with a traditional enveloping method (without response notching) results in a reaction force during the test that is 2.3 (or 3400/1500) times higher than at the coupled system level. With FLV, the input acceleration at the test article resonance frequency would be notched to reduce the shaker force by a scale of 2.3 to the value of 1500 KN, which is the maximum force produced at the coupled system level.

However energy in a test configuration is obtained and the stress peaks at one of the resonance frequency of the test system, occurring at the bottom platform taking place at 28.766 Hz. This also shows a notch value of 12.5 which is quite greater to 2.3 value of the FLV at the support.

It may be noted that our method gives a conservative value which is acceptable. This five times order of magnitude of conservatism in our engineering procedure is mainly due to the simplified text book example of modeling of the system made in the case of prediction of couple interface force.

Chapter Seven: Discussion and Conclusions

In this chapter a general discussion on the results is presented, the important conclusions are listed and some suggestions for further investigations are given.

7.1 Observations and Discussion

The work presented mainly concerns with vibration over testing problem alleviation method by energy limiting vibration approach. The force limiting vibration method is very similar to that of energy limiting but the complexity of the method is much more.

7.2 Conclusions

In spite of the many successful applications of force limiting, a number of interesting research problems remain. Some problems of current interests are: obtaining flight vibratory force data for validation of the technique, calculating and measuring moment impedances, combining multipoint impedances, and assessing errors associated with force measurements. Therefore the following conclusions can be drawn from the present study in an effort to evolve a new and better method.

- ANSYS is effective software and has analytical techniques to predict the vibratory flight energy limits based on the acceleration specification.
- The analysis of the satellite structure confirmed that the energy limiting vibration method is comparative with other methods while significantly notch the amount of over testing. For the analysis a reduction of the response energy with a scale of up to 30 was achieved.
- The energy limiting minimizes the risk of over testing and the associated failures, cost penalties, and schedule delays. In addition, more and better science can be flown for fixed costs, because the hardware need not be over designed for artificial tests.
- The energy prediction depends less or not at all on the flight data and experiments. First, since the energies at critical points are predicted based on von misses stress, thus they can be predicted analytically with more confidence since it is safe from structural failure.

- The strain gauges to measure the stresses in vibration tests are commercially available and make the method easy to apply because it can be put in every critical place regardless of its accessibility.
- The conventional vibration controllers can be conveniently used for energy limiting.
- Although this work was aimed at the evaluation of the method for its application to space satellite, it is clear that the same conclusions apply to a whole range of hardware.

7.3 Suggestions for Future Work

Some of the suggestions for further investigations are:

- To see the application of energy limiting to random vibration testing weather it is straight forward and beneficial for minimizing over testing of the test item.
- To verify the method through an experiment in a controlled laboratory set up to see its ease of application and effectiveness to notching.
- To check the method for composite structure.
- And to make parametric study for the shaker table to get the specimen specific calibration used for the correction of test result.

Appendix A. Derivation of Notch Value for an Element

Stress distribution over a rectangular element is as shown it fig. A.1

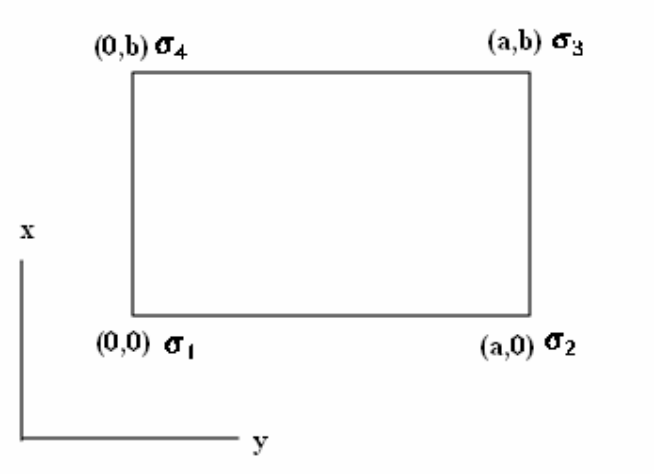

Figure A.1 stress distribution over an element

Assuming a polynomial function of variables x and y

$$\sigma_i(x,y) = a_0 + a_1 x + a_2 y + a_3 xy \qquad \text{A.1}$$

For (x,y) = (0,0) we have

$$\sigma_i(0,0) = a_0 = \sigma_1$$

Therefore

$$a_0 = \sigma_1 \qquad \text{A.2}$$

And for (x,y) = (a,0) we have

$$\sigma_i(a,0) = a_0 + a_1 a = \sigma_2$$

Substituting eq. (A.2) into it and solving it will be

$$a_1 = \frac{\sigma_2 - \sigma_1}{a} \qquad \text{A.3}$$

And for (x,y) = (0,b) we have

$$\sigma_i(0,b) = a_b + a_2 b = \sigma_4$$

Substituting eq. (A.2) into it and solving it will be

$$a_{2=} \frac{\sigma_4 - \sigma_1}{a} \quad \text{A.4}$$

And for (x,y) = (a,b) we have

$$\sigma_i(a,b) = a_0 + a_1 a + a_2 b + a_3 ab = \sigma_3$$

Substituting eq. (A.2), (A.3) & (A.4) into it and solving it will be

$$a_{3=} \frac{\sigma_1 - \sigma_2 + \sigma_3 - \sigma_4}{ab} \quad \text{A.5}$$

Substituting eq. (A.2), (A.3), (A.4) & (A.5) into (A.1) it will be

$$\sigma_i(x,y) = \sigma_1 + \left(\frac{\sigma_2 - \sigma_1}{a}\right)x + \left(\frac{\sigma_4 - \sigma_1}{a}\right)y + \left(\frac{\sigma_1 - \sigma_2 + \sigma_3 - \sigma_4}{ab}\right)xy \quad \text{A.6}$$

Therefore the applied strain energy to the element is

$$U_{ap.} = \frac{t}{E}\int_0^a \int_0^b \left[\sigma_1 + \left(\frac{\sigma_2 - \sigma_1}{a}\right)x + \left(\frac{\sigma_4 - \sigma_1}{a}\right)y + \left(\frac{\sigma_1 - \sigma_2 + \sigma_3 - \sigma_4}{ab}\right)xy\right]^2 dxdy \quad \text{A.7}$$

But the specific strain energy is by substituting the yield stress σ_{yi} for the stresses, so it will be

$$U_{sp} = \left(\frac{t * a * b}{E}\right)\sigma_{yi}{}^2 \quad \text{A.8}$$

It is assumed that the overall reduction in input energy of the shaker table to the test item during testing can be estimated by calculating for the single element.

Therefore the scale of notching is:

$$U_{ap.}/U_{sp} \quad \text{A.9}$$

Appendix B. Prediction of Notch Value for the Critical Elements

The stress distribution of the elements has a form of Fig. A.1. It is summarized in the table below and the data are collected from ANSYS for each element.

Element of critical locations	a(m)	b(m)	t(m)	σ_1(Pa)	σ_2(Pa)	σ_3(Pa)	σ_4(Pa)
1	0.0125	0.025	0.0025	10.6e8	0.66e8	0.323e8	0.466e8
2	0.0125	0.025	0.0025	1.75e8	2.077e8	12e8	12.167e8
3	0.0125	0.025	0.0025	1.822e8	2.16e8	11.96e8	12.10e8
4	0.0125	0.025	0.006	7.975e8	1.855e8	13.1e8	17.9e8
5	0.025	0.025	0.004	7.57e8	0.430e8	1.22e8	2.03e8
6	0.025	0.025	0.0025	0.891e8	0.225e8	7.0154e8	7.02e8

Table B.1 Data for Critical Elements

For 1st Element

Substituting the constants from table B.1 and E of 72.45e9 Pa into eq. A.7 the applied energy is:

$$U_{ap.} = \frac{25}{72.45} \times 10^3 \int_0^{.0125} \int_0^{.025} [10.6 - 795.2x - 405.36y - 31350.4xy]^2 \, dxdy$$

For the double integration a MATLAB is used with a built-in function of dblquad. Therefore the syntax used is as follow:

```
F= @(x,y)(10.6-(795.2*x)-(405.36*y)-(31350.4*x*y)).^2;
Q = dblquad(F,0,.0125,0,.025);
```

$U_{ap.}$ =Q*(25/72.45)*10^3

Therefore MATLAB has given us

$U_{ap.}$ = 2.225 J

And for the specific energy we use eq. (A.8), therefore

$$U_{sp} = \left(\frac{1.25 * 2.5 * 2.5}{72.45}\right) * 200^2 * 10^{-4} = 0.216j$$

Therefore the notch scale will be

$$U_{ap.}/U_{sp} = 10$$

Note that the same procedure is used and table 6.2 is produced.

References

1. Blake, R. E., “The Need to Control the Output Impedance of Vibration and Shock Machines”, Shock and Vibration Bulletin, No. 23, June 1956, pp. 59–64.
2. Morrow, C. T., “Application of Mechanical Impedance Concept to Shock and Vibration Testing”, Los Angeles, CA, TRW Report AD 608030, 1960.
3. O’Hara, G. J., “Mechanical Impedance and Mobility Concepts”, J. of the Acoust. Soc. Am. 41(5), 1967.
4. Rubin, “Mechanical Immitance and Transmission-matrix Concepts”, J. Acoust. Soc. Am. 41(5), 1967.
5. Ratz, A. G., “An Impedance Compensated Random Equalizer”, Proceedings of the Institute of Environmental Sciences 12th Annual Technical Meeting, San Diego, April 1966, pp.353–357.
6. Scharton, T. D., “Development of Impedance Simulation Fixtures for Spacecraft Vibration Tests”, Shock and Vibration Bulletin, No. 40, Pt. 3, 1969, pp. 230–256.
7. Martini, K. H., “Multicomponent Dynamometers Using Quartz Crystals as Sensing Elements”, ISA Transactions, Vol. 22, No. 1, 1983.
8. Salter, J. P. , “Taming the General-Purpose Vibration Test”, Shock and Vibration Bulletin, No. 33, Pt. 3, March 1964, pp. 211–217.
9. Heinricks, J. A., “Feasibility of Force-Controlled Spacecraft Vibration Testing Using Notched Random Test Spectra”, Shock and Vibration Bulletin, No. 36, Pt. 3, Jan. 1967.
10. McCaa, R. and Matrullo, M. “Flight Level Vibration Testing of a Lifting Body Reentry Vehicle”, Shock and Vibration Bulletin, No. 36, Pt. 3, Jan. 1967.
11. Painter, G. W., “Use of Force and Acceleration Measurements in Specifying and Monitoring Laboratory Vibration Tests”, Shock and Vibration Bulletin, No. 36, Pt. 3, Jan. 1967.
12. Murfin, W. B., “Dual Specification in Vibration Testing”, Shock and Vibration Bulletin, No. 38, Pt. 1, 1968.
13. Witte, A. F. and Rodeman, R., “Dual Specification in Random Vibration Testing, an Application of Mechanical Impedance”, Shock and Vibration Bulletin, No. 41, Pt. 44, 1970, pp. 109–118.

14. Hunter, N.F. and J. V. Otts, “The Measurement of Mechanical Impedance and Its Use in Vibration Testing”, Shock and Vibration Bulletin, No. 42, Pt. 1, 1972, pp. 79–88.
15. Witte, A. F., “Specification of Sine Vibration Test Levels Using a Force-Acceleration Product Technique”, Shock and Vibration Bulletin, No. 41, Pt. 4, 1970, pp. 69–78. B-2
16. Wada, B. K., R. Bamford, and J. A. Garba, “Equivalent Spring-Mass System: A Physical Interpretation”, Shock and Vibration Bulletin, No. 42, Pt. 5, 1972, pp. 215–225.
17. Sweitzer, K. A., “A Mechanical Impedance Correction Technique for Vibration Tests”, Proceedings of the Institute of Environmental Sciences 33rd Annual Technical Meeting, 1987, pp. 73–76.
18. Judkins, N. J. and S. M. Ranaudo, “Component Internal Vibration Response Accelerations—System Level versus Component Level”, Proceedings of the 10th Aerospace Testing Seminar, 1987, pp. 97–104.
19. Piersol, A. G. , P. H. White, J. F. Wilby, P. J. Hipol, and E. G. Wilby, “Vibration Test Procedures For Orbiter Sidewall-Mounted Payloads: Phase I Report Appendices”, Astron Research and Engineering (Santa Monica, CA), Rept. 7114-01, 1988.
20. Scharton, T. D. and D. L. Kern, “Using the VAPEPS Program to Support the TOPEX Spacecraft Design Effort”, Proceedings of the 59th Shock and Vibration Symposium, 1988, pp. 21–36.
21. Scharton, T. D., Boatman, D. J. and Kern, D. L., “Dual Control Vibration Testing”, Proceedings of the 60th Shock and Vibration Symposium, 1989, pp.199–217.
22. Scharton, T. D., “Analysis of Dual Control Vibration Testing”, Proceedings of the Institute of Environmental Sciences 36th Annual Technical Meeting, 1990, pp. 140–146.
23. Scharton, T., Force Limited Vibration Testing at JPL, Proceedings of the 14th Aerospace Testing Seminar, Aerospace Corp., Manhattan Beach, Ca., March 1993
24. Scharton, T. D., “Force Limits for Vibration Tests”, CNES Conference on Spacecraft Structures and Mechanical Testing, Paris, FR, June 1994, p. 1024.
25. Scharton, T. D., “Vibration-Test Force Limits Derived From Frequency-Shift Method”, AIAA Journal of Spacecraft and Rockets 32(2), 1995, pp. 312–316.

26. Scharton, T.D., and Chang, K., "Force Limited Vibration Testing of the Cassini Spacecraft and Instruments", IES 17th Aerospace Testing Seminar, Los Angeles, Ca., Oct. 14, 1997.
27. Scharton, T.D., "Frequency-Averaged Power Flow into a One-Dimensional Acoustic System", J. Acoust. Soc. Am., 50 (1), 1971, pp. 374.
28. Smallwood, D. O., "An Analytical Study of a Vibration Test Method Using Extremal Control of Acceleration and Force", Proceedings of the Institute of Environmental Sciences 35th Annual Technical Meeting, 1989, pp. 263–271.
29. Smallwood, D. O., "Development of the Force Envelope for an Acceleration/Force Controlled Vibration Test", Proceedings of the 61st Shock and Vibration Symposium, 1990, pp. 95–104.
30. R. Robert Stevens, "Development of a Force Specification for a Force-Limited Random Vibration Test", 16th Aerospace Testing Seminar, 1996.
31. Daniel B. and Worth A1, "A Method for Implementing Force-Limited Vibration Control", Vol. 40, 1997, pp. 34-41.
32. Daniel B. Worth, and Daniel S. Kaufman, "Validation of Force-Limited Vibrating Testing", Journal of the IEST, Vol. 41, No. 3, 1998, pp. 17-23.
33. Deborah Amato, David Pankow, Knud Thomsen, and Paul Scherrer, "Force Limited Vibration Test of HESSI Imager", NASA Goddard Space Flight Center Greenbelt, Maryland, USA, 2000.
34. Y. Chang, 1997, "Force Limited Vibration Testing the Spacecraft and Instruments" URL: http://www.jpl.nasa.gov/techreport/1997/1997-abs.html
35. Ceresetti, A., "Vibration Over testing on Space H/W due to Shaker Mechanical Impedance, European Conference on Spacecraft Structures, Materials and Mechanical Testing", Noordwijk, ESA-SP-468, 2001, pp.433.
36. J.-C. Salvignol, and O. Brunner, "A New Force Method Device for Spacecraft Testing", ESA Bulletin 105, Feb. 2001, pp.87-90.
37. D. Spanos, and Gregory L. Davis, "A Perspective on the Vibration Over Test Problem", Journal of the Shock and Vibration Digest, Vol. 33, No. 3, 2001, pp. 177-186.
38. Y. Soucy, and A. Cote, "Reduction of Over testing during Vibration Tests of Space Hardware", Canadian Aeronautics and Space Journal, Vol. 48, No. 1, 2002, pp. 77-86.

39. Andre Cote, Ramin Sedaghati, and Yvan Soucy, “Force-Limited Vibration Complex Two-Degree of-Freedom System Method, American Institute of Aeronautics & Astronautics Journal, Vol. 42, No. 6, June 2004.
40. Y. Soucy, V. Dharanipathi and R. Sedaghati, “Investigation of Force-Limited Vibration for Reduction of Over testing”, Journal of Spacecraft and Rockets, Vol.43, No.4, July–August 2006.
41. T.D. Scharton, May 1997 “Force Limited Vibration Testing Monograph”, URL: http://trs-new.jpl.nasa.gov/dspace/bitstream /2014/22483/1/97-0977.pdf
42. Craig L. Stevens, 2002, “Design, Analysis, Fabrication, and Testing of a Nano-satellite Structure”, URL: http://scholar.lib.vt.edu/theses/available/etd-05302002-161341 /unrestricted/clsthesis.pdf